Published in final edited form as:

Nat Med. 2014 August ; 20(8): 886–896. doi:10.1038/nm.3639.

GABA from reactive astrocytes impairs memory in mouse models of Alzheimer's disease

Seonmi Jo[1,2,13], **Oleg Yarishkin**[2,13], **Yu Jin Hwang**[3], **Ye Eun Chun**[2,4], **Mijeong Park**[4,5], **Dong Ho Woo**[2], **Jin Young Bae**[6], **Taekeun Kim**[2], **Jaekwang Lee**[2], **Heejung Chun**[2], **Hyun Jung Park**[7], **Da Yong Lee**[2], **Jinpyo Hong**[2], **Hye Yun Kim**[3], **Soo-Jin Oh**[5], **Seung Ju Park**[2], **Hyo Lee**[2], **Bo-Eun Yoon**[2], **YoungSoo Kim**[3], **Yong Jeong**[8], **Insop Shim**[7], **Yong Chul Bae**[6], **Jeiwon Cho**[4,5], **Neil W Kowall**[9,10,11], **Hoon Ryu**[3,9,10,11], **Eunmi Hwang**[2], **Daesoo Kim**[1], **C Justin Lee**[2,4,5,12]

[1]Department of Biological Sciences, Korea Advanced Institute of Science and Technology (KAIST), Daejeon, Republic of Korea.

[2]WCI Center for Functional Connectomics, Brain Science Institute, Korea Institute of Science and Technology (KIST), Seoul, Republic of Korea.

[3]Center for Neuro-Medicine, Brain Science Institute, KIST, Seoul, Republic of Korea.

[4]Neuroscience Program, Korea University of Science and Technology, Daejeon, Republic of Korea.

[5]Center for Neuroscience, Brain Science Institute, KIST, Seoul, Republic of Korea.

[6]Department of Anatomy and Neurobiology, School of Dentistry, Kyungpook National University, Daegu, Republic of Korea.

[7]Department of Science in Korean Medicine, Graduate School, College of Korean Medicine, Kyung Hee University, Seoul, Republic of Korea.

[8]Department of Bio and Brain Engineering, KAIST, Daejeon, Republic of Korea.

[9]Boston University Alzheimer's Disease Center, Boston University School of Medicine, Boston, Massachusetts, USA.

[10]Department of Neurology, Boston University School of Medicine, Boston, Massachusetts, USA.

[11]VA Boston Healthcare System, Boston, Massachusetts, USA.

Correspondence should be addressed to C.J.L. (cjl@kist.re.kr) or D.K. (daesoo@kaist.ac.kr).

AUTHOR CONTRIBUTIONS

S.J., O.Y., D.K. and C.J.L. designed the study, analyzed the data and wrote the manuscript. O.Y. carried out most slice electrophysiology. Y.J.H., N.W.K. and H.R. performed human tissue experiments. Y.E.C. and D.H.W. performed sniffer patch. S.J., M.P. and J.C. performed behavior tests. J.Y.B. and Y.C.B. performed electron microscopy experiments. S.J., J.L. and H.C. contributed to GABA recording. H.J.P. and I.S. performed microdialysis and HPLC. E.H., D.Y.L. and J.H. contributed to molecular biology. H.Y.K. and Y.K. synthesized $A\beta_{42}$ and performed oligomer western blotting. B.-E.Y. contributed to lentiviral *Maob* shRNA cloning. Y.J. contributed to discussion and to mouse breeding. S.J. conducted all the rest of the experiments with assistance from T.K., S.-J.O., S.J.P. and H.L. All authors contributed to analysis and discussion of the results.

Note: Any Supplementary Information and Source Data files are available in the online version of the paper.

COMPETING FINANCIAL INTERESTS

The authors declare no competing financial interests.

[12]KU-KIST Graduate School of Converging Science of Technology, Korea University, Seoul, Republic of Korea.

[13]These authors contributed equally to this work.

Abstract

In Alzheimer's disease (AD), memory impairment is the most prominent feature that afflicts patients and their families. Although reactive astrocytes have been observed around amyloid plaques since the disease was first described, their role in memory impairment has been poorly understood. Here, we show that reactive astrocytes aberrantly and abundantly produce the inhibitory gliotransmitter GABA by monoamine oxidase-B (Maob) and abnormally release GABA through the bestrophin 1 channel. In the dentate gyrus of mouse models of AD, the released GABA reduces spike probability of granule cells by acting on presynaptic GABA receptors. Suppressing GABA production or release from reactive astrocytes fully restores the impaired spike probability, synaptic plasticity, and learning and memory in the mice. In the postmortem brain of individuals with AD, astrocytic GABA and MAOB are significantly upregulated. We propose that selective inhibition of astrocytic GABA synthesis or release may serve as an effective therapeutic strategy for treating memory impairment in AD.

AD is the most common cause of dementia and is characterized by a progressive decline of memory and other cognitive functions[1]. To date, the causes of memory impairment have been extensively investigated, and the proposed mechanisms include neuronal death induced by β-amyloid (Aβ) oligomer toxicity, glutamate excitotoxicity, oxidative stress[2], synaptic dysfunction by Aβ[3], and tau pathology[4]. Whereas neuronal death has taken center stage in many previous studies, a possible role of glia in memory impairment has been generally overlooked. However, in the brains of subjects with AD, glia undergo prominent changes in morphology and gene expression[5]. Astrocytes become reactive, particularly around amyloid plaques, as indicated by a hypertrophy of the main processes and increased glial fibrillary acidic protein (GFAP) expression[6,7]. Moreover, astrocytes of Alzheimer's model mice show an elevated resting Ca^{2+} level, more frequent Ca^{2+} transients and enhanced intercellular Ca^{2+} waves[8], all of which may potentially lead to an enhanced release of various gliotransmitters, such as glutamate, d-serine, ATP and GABA[9–12]. Consequently, changes in gliotransmitter release are expected after reactive astrocytosis in AD, but to date, this research avenue has not been extensively explored.

Among these gliotransmitters, GABA is the major inhibitory transmitter in the adult mammalian brain[13], and subjects with AD show elevated GABA levels in their cerebrospinal fluid[14], although the mechanism of GABA elevation is unknown. In Alzheimer's model mice, administration of the $GABA_A$ receptor antagonist was shown to improve hippocampal long term potentiation and memory[15], suggesting that aberrant GABAergic inhibition impairs memory in patients with AD. However, antagonizing GABA receptors would not be an effective method of treatment owing to the risk of seizures. If the source of elevated GABA in the cerebrospinal fluid is found, this source could be specifically targeted for treatment. We recently reported that high levels of GABA are tonically released from glia in the cerebellum through Ca^{2+}-activated, GABA-permeable bestrophin 1 (Best1) channels[12],

whereas a low level of tonic GABA release is observed in the hippocampus under normal conditions[16]. Therefore, we hypothesized that an abnormal increase in tonic GABA release from reactive astrocytes in the hippocampus may be directly responsible for the memory impairment in AD.

To investigate this issue, we examined APP/PS1 mice, a widely used model of AD in which the mice carry mutations in amyloid precursor protein and γ-secretase. These mutations are associated with familial AD in humans[17]. As they grow older, APP/PS1 mice show similar pathological characteristics to humans with AD, such as amyloid plaques, reactive astrocytes in the brain[18] and impaired spatial learning and memory[19], without significant neuronal loss[20]. To circumvent the possible limitations of using only one model of APP/PS1, we also employed the 5XFAD mouse model, a primary cell culture system and human tissue samples.

RESULTS

Tonic GABA release is aberrantly increased

First, we investigated the time course of amyloid deposition and the presence of reactive astrocytes in the hippocampus of APP/PS1 mice. Thioflavin-S staining showed that plaques began to appear at the age of 4 months (Supplementary Fig. 1a,b). Although the number of plaques grew with age (Supplementary Fig. 1b), most were concentrated in the lacunosum moleculare and the dentate gyrus (DG) before the age of 11 months (Fig. 1a and Supplementary Fig. 1c,d). At all ages, numerous reactive astrocytes were clustered around the amyloid plaques (Supplementary Fig. 2a,b). Other studies consistently report that DG is one of the first and most plaque-deposited areas both in Alzheimer's model mice and in the brains of subjects with AD[20–22]. DG is known as the principal gateway of cortical input to the hippocampus and is critical for the formation and recall of memory[23,24]. In DG of APP/PS1 mice, neuronal death was not detected at all until 12 months of age[21], even though cognitive impairments were readily observed as early as 8 months of age[25]. Consistent with a previous study[21], we confirmed that at the age of 11 or 12 months, APP/PS1 mice showed no sign of neuronal death in their hippocampus, including DG (Supplementary Fig. 1e). For this reason, we focused our efforts on DG, where we observed many reactive astrocytes before 12 months of age with no observed neuronal death.

To determine whether GABA levels are altered in APP/PS1 mice, we collected interstitial fluid samples from DG of freely moving APP/PS1 mice and wild-type littermates by microdialysis, which enables minimally invasive sampling *in vivo* (Fig. 1b). HPLC analysis of the samples revealed that APP/PS1 mice showed significantly elevated GABA levels when compared with their wild-type littermates (Fig. 1b). Glutamate levels were unaltered (Fig. 1b).

In the central nervous system, GABA has two distinct modes of release: phasic and tonic. Phasic release refers to synaptic release from presynaptic terminals. Tonic release is a sustained form of inhibition[13], which was recently demonstrated to be mediated by astrocytic release through the Best1 channel[12]. To discover whether elevated GABA levels in DG are due to an increase in phasic or tonic release, we performed whole-cell voltage-clamp

recordings from granule cells of DG. To isolate $GABA_A$ receptor–mediated currents, we made the recordings in the presence of the ionotropic glutamate receptor antagonists d-AP5 and CNQX (Fig. 1c), as described previously[12]. We found that the frequency and amplitude of spontaneous inhibitory post-synaptic currents (sIPSCs) were not altered in APP/PS1 mice compared to wild-type littermates (Fig. 1d). However, the tonic current, revealed by blocking with bicuculline (100 μM), was significantly larger in APP/PS1 mice (Fig. 1e). These findings suggest that an aberrant elevation of GABA levels in DG of APP/PS1 mice might be responsible for the increase in tonic GABA current.

Reactive astrocytes abnormally release GABA

Under normal conditions, cerebellar astrocytes contain high levels of GABA, whereas hippocampal astrocytes contain very little GABA, and the amount of astrocytic GABA positively correlates with the degree of tonic inhibition[16]. We used immunostaining procedures with antibodies against GABA[12,16] to determine whether an aberrant increase in tonic GABA current originates from astrocytes in DG, as in the cerebellum. We found that normal astrocytes in wild-type mice showed minimal immunoreactivity for GABA, whereas reactive astrocytes in APP/PS1 mice were strongly immunoreactive (Fig. 1f,g). In the molecular layer of DG, the content of astrocytic GABA increased by a factor of 5 in APP/PS1 mice (Fig. 1h), along with a significant increase in immunoreactivity for Gfap (Fig. 1h). We confirmed the increased Gfap immunoreactivity in APP/PS1 mice by western blot analysis of the tissue homogenates from isolated dentate gyri (Fig. 1i). The intensity of neuronal GABA did not change significantly (Fig. 1g,h). Moreover, the intensity of immunoreactivity for GABA in reactive astrocytes was as strong as that of GABAergic interneurons (Fig. 1g). We consistently observed abundant GABA immunostaining in reactive astrocytes in other regions of the hippocampus, wherever and whenever amyloid plaques were present (Fig. 1f and Supplementary Fig. 2a,b). We did not observe GABA immunoreactivity in other cell types, such as microglia (Supplementary Fig. 2c). We assessed the relationship between the distance from amyloid plaques and astrocytic GABA immunoreactivity by drawing circles of increasing diameter from the center of an amyloid plaque and analyzing the GABA intensity of Gfap-positive astrocytes within each circle (Fig. 1j). We found that astrocytic GABA immunoreactivity inversely correlated with the distance from amyloid plaques, within a distance ranging from 20 to 80 μm (Fig. 1j). Beyond 80 μm, it decreased to the level of astrocytes from wild-type mice (Fig. 1j). We observed a similar increased Gfap and GABA immunoreactivity in another AD model, 5XFAD mice, in which five familial AD-associated mutations are introduced (Supplementary Fig. 2d).

To confirm whether the GABA found in reactive astrocytes is able to be released, we acutely dissociated astrocytes from hippocampal slices and made direct measurements of GABA release from single astrocytes using the sniffer-patch technique[9]. Upon stimulation with TFLLR, a well-characterized peptide agonist for protease-activated receptor-1 (Par1), which increases intracellular Ca^{2+} in astrocytes[9], we detected GABA release with a whole-cell patch-clamped sensor cell expressing $GABA_C$ receptors[12] (Fig. 2a,b). TFLLR-induced GABA release from astrocytes of APP/PS1 mice was significantly higher (Fig. 2c) and more frequently observed (Fig. 2c) compared to that seen in astrocytes of wild-type

littermates. Furthermore, TFLLR-induced GABA release from astrocytes of APP/PS1 mice was completely blocked by pretreatment with natriuretic peptide B (NPPB), an anion channel blocker (Fig. 2b,c), suggesting that GABA release from reactive astrocytes might be mediated by GABA-permeable, NPPB-sensitive Best1 channels[12].

In the cerebellum, Best1 channels are localized in the cell body and processes of Bergmann glia, and they release GABA[12]. In the hippocampus, Best1 is highly expressed at the astrocytic microdomains near synapses and releases glutamate to activate neuronal NMDA receptors that are synaptically localized[9,26]. Thus, we first checked the mRNA expression level of mouse *Best1* in DG and found that *Best1* mRNA expression in APP/PS1 mice was similar to that in wild-type mice (Fig. 2d). However, when we investigated the expression pattern of the Best1 channel in astrocytes of DG, we found markedly different distribution patterns of this channel: in wild-type littermates, we found numerous occurrences of intense punctate staining, which was mostly in the microdomains of astrocytes as previously reported[9,27], whereas in APP/PS1 mice, reactive astrocytes exhibited a remarkably decreased intensity and fewer instances of punctate staining in microdomains (Fig. 2e). Immunogold electron microscopic labeling gave similar results, confirming the markedly decreased Best1 expression in microdomains in APP/PS1 mice (Fig. 2f). Thus, Best1 seems to be redistributed to the soma and processes of reactive astrocytes for possible release of GABA in DG.

GABA synthesis by Maob

The increased GABA levels in reactive astrocytes could be due to elevated GABA production or a reduction in the catabolism or breakdown of GABA. To evaluate these possibilities, we examined levels of glutamate decarboxylase (Gad), which is essential for the production of GABA in GABAergic neurons. Using antibodies against two isoforms of Gad, Gad67 and Gad65, we found that Gad is minimally expressed in reactive astrocytes of APP/PS1 mice (Supplementary Fig. 3a,b,e,f). Besides Gad, GABA can also be produced by the degradation of putrescine, as previously reported in the brain and in cultured astrocytes[28,29]. With antibodies raised against putrescine, we detected increased immunoreactivity in APP/PS1 brain, especially around amyloid plaques (Supplementary Fig. 4a), some in Gfap-positive astrocytes (Supplementary Fig. 4a,c) but mostly in Iba1-positive microglia (Supplementary Fig. 4b,d). Of the three enzymes known to be involved in the putrescine degradation pathway[30] (Supplementary Fig. 4e), Maob is the key enzyme[31], and its activity has been shown to be increased in the postmortem brains of subjects with AD[32,33]. Maob is predominantly expressed in astrocytes in the hippocampus[34] and primarily found in the mitochondria of astrocytes[35]. We observed that reactive astrocytes of APP/PS1 mice showed an increase in Maob expression compared to wild-type astrocytes (Fig. 3a and Supplementary Fig. 4f,g), whereas Maoa expression remained unaltered (Supplementary Fig. 3c,g).

To determine whether Maob activity is enhanced in APP/PS1 mice, we performed a colorimetric assay for Maob (Fig. 3b). We separated subregions of the hippocampus by cutting acutely isolated hippocampi and prepared a mitochondria-rich fraction from tissue homogenates (Fig. 3b). In the DG samples, Maob activity was significantly elevated in

APP/PS1 mice, whereas the Ammon's horn (cornu ammonis, CA) region and whole hippocampus showed no significant difference (Fig. 3c). We investigated the possible role of Maob in GABA production in reactive astrocytes with the use of a selective and irreversible inhibitor of Maob, selegiline[36]. This inhibitor has been approved by the US Food and Drug Administration (FDA) and is prescribed to patients with Parkinson's disease. We chose selegiline over another potent Maob inhibitor, rasagiline, because rasagiline is known to stimulate α-secretase activity[37], which would make the results difficult to interpret. We discovered that drinking-water administration of selegiline at 10 mg kg^{-1} d^{-1} for 3 d completely blocked Maob activity without significantly affecting Maoa activity (Supplementary Fig. 4h–j). In addition, western blot analysis of Aβ in APP/PS1 mice revealed that selegiline in drinking water did not significantly alter the level of Aβ monomer or oligomer compared to drinking water control (Supplementary Fig. 5j). We then assessed GABA levels in reactive astrocytes of APP/PS1 mice after oral administration of selegiline. We found that immunoreactivity for GABA was significantly decreased in Gfap-positive astrocytes of selegiline-treated APP/PS1 mice compared to water-only controls (Fig. 3d,e). We then tested whether inhibition of Maob has any effect on TFLLR-induced GABA release from acutely dissociated astrocytes detected by the sniffer-patch technique (Fig. 2a). We found that a 2-h incubation of acutely dissociated astrocytes of APP/PS1 mice with selegiline completely eliminated the TFLLR-induced GABA release (Fig. 3f,g). These results strongly suggest that the Maob-mediated putrescine degradation pathway is responsible for GABA production in reactive astrocytes.

We next compared the expression of the GABA-catabolizing enzyme, GABA transaminase (Abat), in APP/PS1 and wild-type mice. Using immunostaining, we found most Abat expression in neurons but minimally in astrocytes (Supplementary Fig. 3d). In addition, APP/PS1 mice showed a similar level of Abat expression in reactive astrocytes compared to wild-type mice (Supplementary Fig. 3d,h). Thus, it appears that elevated GABA production is responsible for the increase in GABA content in reactive astrocytes. However, it is unlikely that GABA uptake by the GABA transporter is the source of GABA in reactive astrocytes because expression of the GABA transporters, Gat1 and Gat3, was not substantially altered in APP/PS1 mice compared to wild-type littermates (Supplementary Fig. 3i,j), consistent with a previous report that showed radioligand binding of GAT1 to be unaltered in the brains of subjects with AD[38].

Putrescine and β-amyloid 1–42 cause Maob-mediated GABA production

To further investigate the molecular mechanism of GABA production and release in relation to β-amyloid 1–42 ($Aβ_{42}$), we performed sniffer-patch experiments in hippocampal astrocytes cultured from neonatal wild-type C57BL/6 mice to measure TFLLR-induced GABA release (Fig. 4a,b). In naive astrocytes, TFLLR caused minimal release of GABA (Fig. 4c). However, after an overnight treatment with 180 μM putrescine, astrocytes showed a considerable release of GABA, which was completely inhibited by co-treatment with 100 nM selegiline (Fig. 4c), indicating that Maob is responsible for GABA production. Next we tested whether H_2O_2, a byproduct of Maob reaction, can directly cause GABA production. Overnight treatment with xanthine and xanthine oxidase, a continuous source of H_2O_2 (ref. 39), could not induce GABA release (Fig. 4c), confirming that the putrescine degradation

pathway, but not oxidative stress-related mechanisms, is crucial for GABA production. After a 5-d treatment with 10 μM $A\beta_{42}$, astrocytes also showed a significant release of GABA (Fig. 4d,e), which was also eliminated by an overnight treatment with selegiline (Fig. 4d,e). There was no additive action of $A\beta_{42}$ and putrescine together compared to $A\beta_{42}$ alone (Fig. 4e), indicating that $A\beta_{42}$ and putrescine share the same mechanism involving Maob. Furthermore, the GABA release was eliminated by *Best1*-targeting shRNA (*Best1* shRNA) but not by control scrambled shRNA in putrescine- or $A\beta_{42}$-treated astrocytes (Fig. 4f–i), indicating that Best1 is responsible for GABA release from hippocampal astrocytes.

Maob inhibitors fully rescue impaired spike probability

Tonic GABA release is known to inhibit neuronal excitability and network activity in various brain regions[13]. Thus, we investigated the possible role of tonic GABA release from reactive astrocytes in synaptic transmission in dentate granule neurons by whole-cell voltage-clamp recordings. First, we tested basal synaptic transmission in acute brain slices by measuring the frequency and amplitude of spontaneous excitatory post-synaptic currents (sEPSCs) and miniature EPSCs (mEPSCs). There was a slightly higher amplitude and considerably lower frequency of sEPSCs and mEPSCs in APP/PS1 mice compared to wild-type mice (Supplementary Fig. 5a–f). Furthermore, we found the amplitude of evoked EPSCs (eEPSCs) was substantially increased in APP/PS1 mice (Supplementary Fig. 5g–i). These results suggest that tonic inhibition by GABA release in APP/PS1 mice results in synaptic scaling[40] by increasing the amplitude of sEPSCs and mEPSCs. GABA, on the other hand, decreases the frequency of sEPSCs, perhaps by decreasing the release probability.

To examine the presynaptic effect of tonic GABA release, we recorded two consecutive eEPSCs, which were separated by varying interstimulation intervals to calculate the paired-pulse ratio (PPR), upon electrical stimulation of perforant path fibers in the molecular layer of DG (Fig. 5a). We found that the PPR was significantly increased in APP/PS1 mice compared to wild-type mice at 50-ms interstimulation interval (Fig. 5a). This increased PPR in APP/PS1 mice was fully rescued to the level of wild-type mice by selegiline pretreatment (Fig. 5a). Taken together, these results suggest synaptic transmission is strongly inhibited by GABA production and release from reactive astrocytes through a presynaptic mechanism involving decreased probability of release in APP/PS1 mice.

To determine the consequence of tonic inhibition on synaptically elicited action potential firing in dentate granule neurons, we performed whole-cell current-clamp recordings and measured the spike probability of synaptically elicited excitatory post-synaptic potentials (EPSPs) upon electrical stimulation of perforant path fibers. Spike probability in APP/PS1 mice was markedly reduced compared to wild-type littermates at stimulation intensities above 100 μA (Fig. 5b), indicative of impaired synaptic probability[41]. The maximum spike probability in APP/PS1 mice never reached a probability of 1, even at the stimulation intensity of 1,000 μA (Fig. 5b), but instead plateaued at a probability of around 0.6 (Supplementary Table 1). This impaired spike probability was almost fully restored by bath application of both the $GABA_A$ receptor antagonist bicuculline and the $GABA_B$ receptor antagonist CGP55845 (Fig. 5c,d), suggesting that GABAergic inhibition is underlying the impaired spike probability in APP/PS1 mice. Furthermore, impaired spike probability in

APP/PS1 mice was fully rescued after oral administration of selegiline for a week (Fig. 5c,d) at a dose that had no apparent effect in wild-type littermates (Supplementary Fig. 6a–d). We found a similar effect of full rescue after direct incubation of slices with selegiline for 2 h (Supplementary Fig. 6e,f). Furthermore, gene silencing of *Maob* or *Best1* by lentivirus carrying *Maob* shRNA or *Best1* shRNA also resulted in full rescue of spike probability compared to the scrambled shRNA in APP/PS1 mice (Fig. 5e,f). The resting membrane potential or input resistance of dentate granule neurons for each test condition and mouse type was not different (Supplementary Table 1). Consistent with the results observed in APP/PS1 mice, 5XFAD mice showed impaired spike probability that could be fully rescued by lentiviral delivery of *Best1* shRNA (Fig. 5g,h). These findings demonstrate that GABA production and tonic release from reactive astrocytes impairs spike probability at the perforant-path-to-dentate-granule-cell synapse and that a blockade of Maob or gene silencing of *Best1* fully rescues the observed impairment.

Maob inhibitor restores synaptic plasticity and memory

We expected that the suppression of spike probability in DG would strongly influence synaptic plasticity and learning and memory-related behaviors. To address the role of tonic GABA release from reactive astrocytes in synaptic plasticity, we recorded eEPSCs from dentate granule neurons before and after a high-frequency stimulation protocol (200 Hz, 40 ms, eight times at 2-s interval) to induce long-term potentiation (LTP). We found that LTP was significantly impaired in APP/PS1 mice compared to wild-type littermates, but it was fully restored by oral administration of selegiline for a week (Fig. 5i).

To address the role of tonic GABA release from reactive astrocytes in hippocampus-dependent learning and memory, we subjected mice to a passive avoidance paradigm, in which they learned to avoid a dark chamber after exposure to an electrical foot shock, followed by a retention test on the next day (Supplementary Fig. 7a). Consistent with a previous report[42], learning and memory was impaired in APP/PS1 mice, as evidenced by a significant reduction in latency to enter the dark chamber (Fig. 5j). Oral administration of selegiline for a week mostly restored the learning and memory impairment of APP/PS1 mice in the passive avoidance paradigm (Fig. 5j and Supplementary Table 2). The increased latency to enter the dark chamber is not likely to be due to enhanced anxiety or depression because selegiline is not anxiogenic[43] and has been approved by the FDA to treat major depression.

Next, we performed the Morris water maze test, which is a widely known test for hippocampus-dependent learning and memory (Supplementary Fig. 7a,b). Consistent with a previous report[42], we found that APP/PS1 mice learned more slowly than did wild-type mice, as evidenced by slower escape latency during the acquisition training days without any difference in swim speed (Supplementary Fig. 7c,d). This learning and memory deficit was partially rescued in APP/PS1 mice after oral administration of selegiline for 14 d before and 15 d during the testing period, a total of 29 d without any change in swim speed (Supplementary Fig. 7c,d and Supplementary Table 2). The only partial rescue shown in Morris water maze performance could be due to the fact that selegiline loses its efficacy when administered over long periods of time[44]. To address this issue, we tested the effect

of selegiline on spike probability of dentate granule neurons by varying the administration period. The spike probability was progressively and significantly decreased after a 2- and 4-week compared to a 1-week administration of selegiline in APP/PS1 mice (Fig. 6a–d). These results could explain why the behavior was not fully rescued in the Morris water maze test.

The short-lived action of selegiline has been previously reported[44,45] and attributed to the irreversibility of its action. To test the idea of reversibility, we assessed the effect of prolonged administration of a reversible Maob inhibitor, safinamide[46]. We found that 2-week administration of safinamide significantly rescued the spike probability at 200-μA stimulation intensity in APP/PS1 mice, even to the untreated wild-type level, whereas 2-week administration of selegiline started to show a wearing-off effect (Fig. 6a–d). These results indicate that, unlike treatment with selegiline, prolonged treatment with a reversible inhibitor shows prolonged efficacy on spike probability.

Increased GABA and MAOB in AD

In order to assess the clinical importance of GABA production in reactive astrocytes, we obtained temporal cortex brain samples from 11 individuals with AD and 11 control human subjects (Supplementary Table 3). The temporal cortex surrounds the hippocampus and is vital for memory function in association with the hippocampus[47]. Using the GABA-specific antibody, we saw an enhanced immunoreactivity for GABA throughout the temporal cortex in samples from individuals with AD, compared to control samples (Fig. 6e). We observed increased GABA immunoreactivity in every layer of the temporal cortex, including both gray matter and white matter, with the greatest increase detected in the peripheral layer (Fig. 6e). We then measured mRNA expression levels of *GFAP* and *MAOB* by performing quantitative real-time PCR. The mRNA expression levels of both *GFAP* (Fig. 6f) and *MAOB* (Fig. 6g) were significantly higher in individuals with AD than in control subjects. We found a positive correlation between *GFAP* and *MAOB* expression (Fig. 6h). Consistent with the mouse model, immunostaining showed a marked increase of GFAP, MAOB and GABA in reactive astrocytes in brain samples from individuals with AD (Fig. 6i). We can thus conclude that reactive astrocytes showing an aberrant increase in MAOB and GABA are also present in individuals with AD.

DISCUSSION

We have investigated here the detailed molecular and cellular mechanisms of GABA synthesis and release in reactive astrocytes of AD model mice (Supplementary Fig. 8). In summary, normal astrocytes do not contain GABA, and Best1 channels are located at microdomains to release glutamate, which targets synaptic NMDA receptors. Diseased astrocytes around amyloid plaques become reactive and produce GABA. Increased production of GABA by Maob is responsible for the marked increase in GABA levels observed in reactive astrocytes. Consequently, GABA is released from reactive astrocytes through the glutamate- and GABA-permeable Best1 channel. Meanwhile, the Best1 channel is redistributed away from microdomains to the soma and processes of reactive astrocytes, possibly switching its target from synaptic NMDA receptors to extrasynaptic GABA

receptors. The released GABA activates neuronal $GABA_A$ and $GABA_B$ receptors, which, in turn, strongly inhibit synaptic release. Thus, GABA from reactive astrocytes diminishes the spike probability of the perforant-path-to-dentate-granule-cell synapse, leading to impairment in synaptic plasticity and memory function. To the best of our knowledge, our study provides insight into the causes of memory impairment in AD: reactive astrocytes are actively involved in glia-neuron interactions, with GABA acting as a gliotransmitter, working in concert with other pathological factors to influence neural networks in diseased brain[48].

Soluble toxic species of Aβ can induce reactive astrocytosis in cultured astrocytes[49]. In addition, several mouse models show cognitive impairment well before the first occurrence of amyloid plaques[50]. Thus, at early stages of disease progression, the soluble toxic species of Aβ, including oligomeric species, might cause cognitive impairment via reactive astrocytosis and GABA production. Consequently, our proposed intervention of blocking astrocytic GABA might be efficacious in a preventive manner at early stages of AD. In support of this idea, our results demonstrate that toxic species of Aβ can cause GABA production without amyloid plaques in cultured hippocampal astrocytes (Fig. 4).

The impairment of LTP in the perforant-fiber-path-to-dentate synapse is in marked contrast to the previously reported unaltered LTP at CA3-CA1 synapses in the same model mice (APP/PS1) at the age of 12–13 months[42]. At this age, animals contain a few amyloid plaques in CA1 (Supplementary Fig. 1a). Notably, that study reported similar behavioral impairments in the passive avoidance task and Morris water maze as in our study, but with no impairment in synaptic transmission at the CA3-CA1 synapse. Therefore, these observations imply that the memory impairment seen in 12- to 13-month-old APP/PS1 mice is probably due to synaptic impairment not in CA1, but in DG, where numerous amyloid plaques and abundant GABA-producing reactive astrocytes are found.

The observed synaptic impairment in DG cannot be explained by impaired surface expression of postsynaptic glutamate receptors such as AMPA receptor (AMPAR)[51]. We observed slightly increased amplitude of AMPAR-mediated sEPSCs, mEPSCs and eEPSCs in APP/PS1 mice (Supplementary Fig. 5), suggesting an enhanced activity of AMPAR in dentate granule neurons. However, the stimulation-induced spike firing decreased markedly in dentate granule neurons, to the point of complete elimination of spikes (Fig. 5b). This indicates that AMPAR does not contribute to the spike probability and cognitive impairment. Instead, we found a strong presynaptic inhibition, via $GABA_A$ and $GABA_B$ receptors, contributing to the spike probability and cognitive impairment (Fig. 5a,d). Inhibition of tonic GABA release by selegiline treatment fully rescued the impairments in spike probability, LTP, and learning and memory (Fig. 5d,i,j), whereas it did not rescue the altered activity of AMPAR, which remained enhanced after selegiline treatment (Supplementary Fig. 5g–i). This implies that there is a lack of correlation between enhanced AMPAR and cognitive impairment. Consistent with this idea, an enlargement of synapses has been observed in AD[52], which has been interpreted as a compensatory response.

Increased tonic GABA release by reactive astrocytes could exert diverse functional effects according to specific regions with specific neuronal networks. In DG, the majority of

synapses near reactive astrocytes are glutamatergic perforant path synapses. Thus, GABA from reactive astrocytes inhibits the activity of dentate granule neurons, resulting in inhibition of spike probability and contributing to learning and memory impairments (Fig. 5). On the other hand, in the case of cortical layer II–III, where GABAergic interneurons are widely distributed[53], GABA from reactive astrocytes could inhibit the activity of interneurons in the vicinity, resulting in disinhibition onto glutamatergic principal neurons and contributing to previously reported epileptiform discharges[54]. Unfortunately, the authors of both reports[53,54] did not measure tonic inhibition, and this idea remains to be tested in the future. Therefore, depending on the brain region in which reactive astrocytes are prevalent, various neurological symptoms can arise in each patient during the progression of AD.

We expect that suppression of GABA production or release from reactive astrocytes would bring about desirable therapeutic effects on memory impairment in AD. Indeed, several studies show the beneficial effects of the MAOB inhibitor selegiline on cognitive impairment in patients with AD[55–57]. Although a meta-analysis study from 17 selegiline trials[58] concluded that there was no justification for using selegiline in the treatment of AD, the same study found some evidence for selegiline's beneficial effects on memory. The mode of action of selegiline, however, has not been fully understood or has never been studied in relation to GABA. Our work offers a clear explanation of the action of selegiline in memory impairment in its inhibition of GABA production in reactive astrocytes. However, selegiline is known to have side effects and short-lived actions[44,45]. It generates neurotoxic metabolites such as l-methamphetamine, which causes psychosis and other side effects[45]. The short-lived action of selegiline[44] (Fig. 6a–d) is perhaps through compensatory mechanisms by Maoa or overexpression of Maob due to the permanent damage to flavin adenine dinucleotide (FAD), a cofactor of Maob[59]. Therefore, the use of drugs like selegiline, which loses its efficacy when administered over long periods, might not be optimal. These obstacles make it clear that there is a pressing need for developing better MAOB inhibitors by changing irreversibility or by optimizing prescription methods. In the future, reversible MAOB inhibitors such as safinamide should be tested in mouse models following longitudinal paradigms, in which potential toxicity due to long-term administration of the drug will be thoroughly evaluated.

Reactive astrocytes are commonly observed not only in AD but also in other brain diseases, such as Parkinson's disease, stroke, epilepsy and traumatic brain injury[7,60]. However, their role has mainly been investigated in the context of inflammation or metabolic support. Our study provides an insight into the role of glia-neuron interactions via GABA in understanding and treating brain diseases. Consistent with this idea, we found that stab-wound injuries caused increased Gfap expression and induction of astrocytic GABA production in the injured area (Supplementary Fig. 9), suggesting that this is a general mechanism for diseases or injuries that accompany reactive astrocytosis. As with GABA, the roles of other gliotransmitters, such as glutamate, d-serine, taurine, glycine and ATP, in AD and in other brain diseases, are awaiting further investigations, offering new challenges for the future.

METHODS

Methods and any associated references are available in the online version of the paper.

ONLINE METHODS

Animals.

Mice had free access to food and water and were kept on a 12-h lightdark cycle. All animals were housed in groups of 3–5 per cage. All animal care and handling was performed according to the directives of the Animal Care and Use Committee of KAIST (Daejeon, Korea) and the Institutional Animal Care and Use Committee of KIST (Seoul, Korea). APPswe/PSEN1dE9 (APP/PS1) mice of B6C3 hybrid background were originated from Jackson Laboratory (USA, stock number 004462) and maintained as hemizygotes by crossing transgenic mice to B6C3 F1 mice. Both sexes of 8- to 13-month-old transgenic mice and wild-type littermates were used. 69 mice were subjected to behavioral tests. For immunogold electron microscopy, APP/PS1 mice were crossed with Gfap-GFP mice (Jackson Laboratory, stock number 003257). 5XFAD mice of B6SJL hybrid background (Jackson Laboratory, stock number 008730) were maintained by crossing hemizygote transgenic mice to B6SJL F1 mice. For stab wound injury, 8- to 11-week-old male C57BL6/J mice were used. For kainic acid injection, 8-week-old male ICR mice were used. For oral administration of selegiline or safinamide, 10 mg of r-(–)-deprenyl hydrochloride (Sigma) or safinamide was dissolved in 150 ml water. The mice were provided with water (control), selegiline or safinamide solution *ad libitum.* Dose was calculated as 5–10 mg kg^{-1} d^{-1}. Behavioral experiments were performed during light phase of the light-dark cycle at the same time of each day. All experiments were done with gender- and age-matched controls. Different sets of mice were used for each experiment except for repeated results in Figure 3f,g and Figure 6a–d.

In vivo microdialysis.

Mice were kept under isoflurane anaesthesia (1.5%) and mounted in a stereotaxic frame (Stoelting). After exposing the skull and drilling a burr hole, a guide CMA7 cannula (CMA Microdialysis) was positioned in the right hippocampus (AP, –1.8 mm; ML, –1.3 mm from bregma; DV, –2.0 mm below the dura)[61] and secured to the skull with anchor screws and acrylic dental cement. Following recovery from anesthesia, a CMA7 microdialysis probe of concentric design (CMA Microdialysis) was inserted through the guide cannula, extending throughout the hippocampus. The probe was connected to a CMA100 microperfusion pump (CMA Microdialysis) with polyethylene (PE-20) tubing and perfused with artificial cerebrospinal fluid (ACSF) composed of (in mM): Na^+ 151.1, K^+ 2.6, Mg^{2+} 0.9, Ca^{2+} 1.3, $C1^-$122.7, HCO_3^- 21.0, HPO_4^{2-} 2.5 and glucose 3.87 at a speed of 1 μl min^{-1}. Perfusates from the outlet end of the tubing were collected in plastic vials standing in ice. Samples were collected over 20 min intervals for 2 h. The second dialysate was used for measurement of l-glutamate and GABA.

L-glutamate and GABA measurement.

1 mg ml^{-1} stock solutions of GABA/glutamate standards were prepared in HPLC-grade water, aliquoted out and stored at –20 °C. Working solutions (1 μg ml^{-1} and 5 μg ml^{-1} for glutamate; 100 ng ml^{-1} and 500 ng ml^{-1} for GABA) were prepared daily by dilutions of those stock solutions, aliquoted out and stored at 4 °C until derivatisation and analysis[62,63]. Briefly, the derivatization was performed by mixing 100 μl *in vivo* microdialysate or standard solutions, 20 μl of daily prepared methanolic *o*-phthalaldehyde (5 mg ml^{-1}), 75 μl borate buffer (pH 9.9) and 5 μl 3-mercaptopropionic acid. The resulting solution was vortexed and analyzed after 1 min at room temperature. The HPLC system consisted of a Waters chromatograph (Waters) with a 200-μl loop (Rheodyne 7725-I) and a fluorescence detector (FLD-Waters spectrofluorometric detector 2475), coupled to an LC-10 AD pump. The system was equipped with a 3-μm particle size (150 mm × 4.6 mm, ID) C18 analytical column (Hibar-Futigsanle RT) and a prepacked column (RT 250–4 E, Merck). An integrator (Empower 2) was used to analyze the chromatographic data. The mobile phase consisted of 0.05 M sodium acetate, tetrahydrofuran and methanol (50:1:49, v:v:v) adjusted to pH 4.0. The mobile phase was filtered through Millipore 0.45-μm Durapore membrane filters and vacuum degassed before use. Chromatographic analyses were performed at 25 ± 2 °C. Compounds were eluted isocratically over a 9-min runtime at a flow rate of 1 ml min^{-1}. The fluorescence detector was set at an excitation wavelength of 337 nm and an emission wavelength of 454 nm, low sensitivity and range GABA/glutamate were identified by their characteristic retention times as determined by standard injections. Sample peak areas were measured through the integrator system and compared with the calibration curve standard in order to quantify the amino acid concentrations.

Cresyl violet staining.

After microdialysis was completed, the position of the dialysis probe was verified by cresyl violet staining. 30-μm-thick coronal cryostat sections were prepared as described later in the immunostaining section, mounted on slides, allowed to dry for 10 min and stained with a cresyl violet solution (Sigma) for 5 min. They were then dehydrated in increasing ethanol concentrations and finally coverslipped from xylene. The lesion site was measured at 100× magnification using a microscope (Olympus). Only those animals in which the probe was correctly located were included in the study.

Sniffer patch from acutely dissociated hippocampal astrocytes.

350-μm-thick horizontal hippocampal slices were obtained in the same way as in tonic GABA recordings. The hippocampal DG region was isolated from each slice and enzymatically dissociated with the tip of a polished Pasteur glass pipette in ASCF, which contained 20 mg ml^{-1} proteinase (type XXIII, Sigma) and was preoxygenated for 30 min. Tissue were incubated for 30 min at 37 °C with oxygenation. Enzyme-treated tissues were washed with ACSF and then triturated with a polished Pasteur glass pipette in a row. Supernatant cells were filtered with Cell Strainer (BD Falcon, 70 μm). Eluted cells were plated on a 0.05 mg ml^{-1} PDL-coated cover glass and placed in an incubator for about 2 h before use. Then HEK 293T cells, originated from Korean Cell Line Bank (Seoul National University, Korea), expressing $GABA_CR$ and EGFP were added onto the cover

glass with acutely dissociated cells[12]. According to a previous report[9], astrocytes can be identified morphologically. To determine whether GFP-expressing HEK 293T cells express $GABA_C$R, 100 μM GABA was bath-applied to induce $GABA_C$R-mediated full current. To block Ca^{2+}-activated Cl^- channel-mediated GABA release, NPPB was pretreated for 5 min. During the sniffer-patch experiment, astrocytic Par1 receptor was activated by pressure application of the Par1 agonist, TFLLR through a glass pipette containing 500 μM TFLLR, positioned near an astrocyte, using Picospritzer (Parker Instrument) for 100 ms at a pressure of 10 p.s.i. Sniffer-patch experiments from acutely dissociated astrocytes were performed within 6 h after plating.

Sniffer patch from primary cultured astrocytes.

Primary hippocampal astrocytes were prepared from P0–P2 of C57BL/6 mice as described[9]. One day before the experiment, HEK 293T cells were transfected with 1:10 ratio of green fluorescence protein (pEGFP-N1) and $GABA_C$ receptor using Effectene (Qiagen). On the day of sniffer patch, HEK 293T cells expressing $GABA_C$ were dissociated, triturated, added onto the cover glass with cultured astrocytes, and then allowed to settle for at least 1 h before sniffer patching. After HEK cells settled, cultured astrocytes were incubated with 5 μM Fura-2AM (mixed with 1 ml of external solution containing 5 μl of 20% pluronic acid, Invitrogen) for 40 min and washed at room temperature and subsequently transferred to a microscope stage. External solution contained (in mM): 150 NaCl, 10 HEPES, 3 KCl, 2 $CaCl_2$, 2 $MgCl_2$, 5.5 glucose, pH adjusted to pH 7.3 and osmolality to 325 mOsmol kg^{-1}. Intensity images of 510-nm wavelength were taken at 340-nm and 380-nm excitation wavelengths using either iXon EMCCD (DV887 DCS-BV, ANDOR technology). The two resulting images were used for ratio calculations in Axon Imaging Workbench version 6.2 (Axon Instruments). During sniffer patch, astrocytic Par1 receptor was activated by pressure application of the Par1 agonist, TFLLR, through a glass pipette containing 500 μM TFLLR, positioned near an astrocyte, using Picospritzer (Parker Instrument) for 100 ms. $GABA_C$-mediated currents were recorded from HEK 293T cells under voltage clamp (V_h = –70 mV) using Axopatch 200A amplifier (Axon Instruments), acquired with pClamp 9.1. Recording electrodes (4–7 MΩ) were filled with (mM): 110 Cs-gluconate, 30 CsCl, 0.5 $CaCl_2$, 10 HEPES, 4 Mg-ATP, 0.3 Na_3-GTP and 10 BAPTA (pH adjusted to 7.3 with CsOH and osmolality adjusted to 290–310 mOsm kg^{-1} with sucrose). For simultaneous recordings, Imaging Workbench was synchronized with pClamp 9.1. To normalize for different amounts of expression of $GABA_C$ receptors on the HEK 293T cells, 100 μM of GABA in the bath was applied to maximally activate the $GABA_C$ receptors after current recording. Normalization was then accomplished by dividing the current induced by GABA released from astrocytes by the current induced by bath application of GABA. $A\beta_{42}$ peptide (H_2N-DAEFRHDSGYEVHHQKLVFFAEDVGSNKGAIIGLMVGGVVIA-COOH) was prepared as previously described[64].

Transfection of *Best1* shRNA.

Before replating onto a cover glass for sniffer patch, cultured astrocytes were transfected with shRNA by electroporation. The pSicoR-*Best1*-shRNA was adopted from a previous report[12] and the complementary oligomers were 5′-TTG CCA ACT TGT CAA TGA ATT CAA GAG ATC ATT GAC AAG TTG GCA ATT TTT TC-3′ and 5′-CGA GAA AAA ATC

GCA TAG CGT ATG CCG TTT CTC TTG AAA ACG GCA TAC GCT ATG CGA A-3′. A scrambled shRNA-containing pSicoR construct was used for controls.

Tonic GABA recording.

$GABA_A$-receptor–mediated current in dentate granule cells was measured as previously described[12]. Mice were deeply anesthetized and decapitated. After decapitation, the brain was quickly excised from the skull and submerged in ice-cold cutting solution that contained (in mM): 250 sucrose, 26 $NaHCO_3$, 10 d-(+)-glucose, 4 $MgCl_2$, 3 myo-inositol, 2.5 KCl, 2 sodium pyruvate, 1.25 NaH_2PO_4, 0.5 ascorbic acid, 0.1 $CaCl_2$ and 1 kynurenic acid, pH 7.4. All solution was gassed with 95% O_2–5% CO_2. The hemisected brain was glued onto the stage of a vibrating microtome (Leica VT1000S) and 300-μm-thick coronal hippocampal slices were cut and transferred to an extracellular ACSF solution: 126 NaCl, 24 $NaHCO_3$, 1 NaH_2PO_4, 2.5 KCl, 2.5 $CaCl_2$, 2 $MgCl_2$, and 10 D-(+)-glucose, pH 7.4. Slices were incubated at room temperature for at least 1 h before recording. Slices were transferred to a recording chamber that was continuously perfused with ACSF solution (flow rate = 2 ml min^{-1}). The slice chamber was mounted on the stage of an upright Olympus microscope and viewed with a 60× water immersion objective (NA = 0.90) with infrared differential interference contrast optics. Cellular morphology was visualized by a CCD camera and Imaging Workbench software (Indec BioSystems). Whole-cell recordings were made from granule cell somata located in DG. The holding potential was –70 mV. Pipette resistance was typically 6–8 MΩ and the pipette was filled with an internal solution: 135 CsCl, 4 NaCl, 0.5 $CaCl_2$, 10 HEPES, 5 EGTA, 2 Mg-ATP, 0.5 Na_2-GTP, 10 QX-314, pH adjusted to 7.2 with CsOH (278–285 mOsmol). Before measuring tonic current, baseline current was stabilized with d-AP5 (50 μM) and CNQX (20 μM). Electrical signals were digitized and sampled at 50-μs intervals with Digidata 1440A and Multiclamp 700B amplifier (Molecular Devices) using pCLAMP10.2 software. Data were filtered at 2 kHz. The amplitude of tonic GABA current was measured by the baseline shift after bicuculline (100 μM) administration using the Clampfit program. Tonic current density was calculated from the current amplitude divided by the membrane capacitance. Frequency and amplitude of spontaneous inhibitory post-synaptic currents (IPSCs) before bicuculline administration was detected and measured by Minianalysis (Synaptosoft).

Evoked spike probability.

Electrophysiological recordings were made from horizontal brain slices of 400-μm thickness. Brain tissue was cut using a Leica VT1000S microtome in oxygenated ice cold ACSF composed of (in mM): 130 NaCl, 2.5 KCl, 26 $NaHCO_3$, 1.25 NaH_2PO_4, 1.0 $CaCl_2$, 3.0 $MgCl_2$, and 10 d-glucose. After slicing, the tissue was maintained at a room temperature of 20–22 °C for at least 60 min in ACSF of the same composition and then transferred to the recording chamber. Recordings were performed at room temperature of 20–22 °C in oxygenated ACSF, contained (in mM): 130 NaCl, 2.5 KCl, 26 $NaHCO_3$, 1.25 NaH_2PO_4, 1.5 $CaCl_2$, 1.5 $MgCl_2$ and 10 d-glucose. Synaptic responses in dentate granule cells were evoked by 0.1 Hz stimulation of lateral perforant path fibers (100 μs duration; 100–1,000 μA intensity) via a constant current isolation unit. Perforant path fibers were stimulated by placing a tungsten bipolar electrode in the outer half of the middle third dentate molecular layer. The evoked EPSPs were recorded using glass pipette electrodes

(6–8 MΩ), filled with intracellular solution contained (in mM): 120 potassium gluconate, 10 KCl, 1 $MgCl_2$, 0.5 EGTA, 40 HEPES (pH 7.2 was adjusted with KOH). Spiking probability was calculated as the ratio of the number of successful (spike-generating) stimulations to the total number of stimulations. Whole-cell patch-clamp recordings, using a Multiclamp7 amplifier (Molecular Devices), were performed from DG granule cells, visually identified with infrared video microscopy and differential interference contrast optics. Data were collected with a Multi-Clamp 700B amplifier (Molecular Devices) using Clampex10 acquisition software (Molecular Devices) and digitized with Digidata 1322A (Molecular Devices). Raw data were low pass filtered at 4 kHz and collected for off-line analysis at a sampling rate of 10 kHz using pClamp10.2 software.

EPSCs and LTP.

Spontaneous EPSCs were measured from recordings of 4–5 min duration. Miniature EPSCs were measured in the presence of 1 μM TTX. Holding potential was set as –70 mV. Pipette solution for evoked and spontaneous EPSC recordings contained (in mM): 140 Cs-methanesulphonate, 8 NaCl, 1 $MgCl_2$, 0.5 EGTA, 10 HEPES, 7 phosphocreatine di(tris) salt, 4 Mg-ATP, 0.3 Na_2-GTP, 5 QX314 (pH7.3 was adjusted with NMDG). LTP was induced with a 200-Hz stimulus for 40 ms. This procedure was performed 8 times at 2-s intervals. Stimulus intensity was adjusted to evoke an eEPSC of approximately 30–40% of the maximal amplitude. Pipette solution for LTP experiments contained (in mM): 140 Cs-methanesulphonate, 8 NaCl, 1 $MgCl_2$, 0.05 EGTA, 0.0244 $CaCl_2$ (100 nM free Ca^{2+} was calculated with Maxchelator (http://maxchelator.stanford.edu/), 10 HEPES, 7 phosphocreatine di(tris) salt, 4 Mg-ATP, 0.3 Na_2-GTP, 5 QX314 (pH7.3 was adjusted with NMDG).

Drugs and chemicals.

QX-314 bromide, (–)-bicuculline methobromide, CGP55845 hydrochloride, d-AP5, CNQX were purchased from Tocris. The synthetic amino acid peptides, TFLLR-NH2, were purchased from Peptron. Pluronic acid (F-127) and Fura-2AM were purchased from Molecular Probe. NPPB and other reagents were purchased from Sigma.

Gene silencing *in vivo*.

The scrambled shRNA– or *Best1* shRNA–expressing lentiviral vector was prepared as previously described[12]. Lentiviral *Maob*-shRNA was prepared in the same way. Mice were deeply anesthetized with 2% avertin (20 μg g^{-1}, i.p.) and mounted in a stereotaxic frame (Kopf). The scalp was incised and a hole drilled into the skull above the hippocampus (AP, –1.7 mm; ML, –1 or +1 mm from bregma) and a hollow glass needle loaded with lentivirus was introduced slowly into the DG (DV, –1.7 mm below the dura)[61]. By using a syringe pump (KD Scientific), 2 μl of virus was injected in both dentate gyri at a rate of 0.2 μl min^{-1}. Evoked spike probability experiments were performed 7 d after viral transduction.

Amyloid plaque staining and counting.

Mice were deeply anesthetized with 2% avertin (20 μg g^{-1}, i.p.) and perfused with 0.9% saline followed by ice cold 4% paraformaldehyde (PFA). Excised brains were post-fixed

overnight in 4% paraformaldehyde at 4 °C and immersed in 30% sucrose for 48 h for cryoprotection. Coronal hippocampal sections were cut at 30 μm in a cryostat and floated in PBS. After 3 additional washes in PBS, sections were used for staining. To visualize amyloid plaques, sections were incubated in 1 mM thioflavin-S, which had been dissolved in 50% ethanol for 8 min. Sections were rinsed with 80% ethanol twice for differentiation and washed with PBS 3 times. The images were taken by an Olympus BX50 microscope and an Olympus DP50 camera with GFP filter set. 400× magnified images containing most part of the hippocampus were used for counting the average number of plaques in hippocampus.

Propidium iodide (PI) staining *in vivo*.

To detect dead cells, PI was administrated as described in the previous study[65] with slight modifications. Briefly, 4 mg kg^{-1} of PI (Sigma) was injected into the tail vein of wild-type and APP/PS1 mice. After 5 h, the mice were killed, and the obtained brain tissues were processed for confocal microscopy imaging. 30-μm-thick sections were mounted on PDL-coated glass slides using DAPI containing mounting medium. As positive and negative controls, seizure mouse models induced by kainic acid (20 mg kg^{-1}, i.p., Sigma) and PBS injected mice were used respectively.

Antibodies.

The primary antibodies used for immunostaining were as follows: chicken anti-Gfap (1:500, Millipore ab5541), rabbit anti-Iba1 (1:500, Wako 019–19741), guinea pig anti-GABA (1:1,000, Millipore ab175), chicken anti-GFP (1:1,000, Abcam ab13970), rabbit anti-Best1 (refs. 12,66) (1:100, custom made), mouse anti-Gad67 (1:1,000, Millipore mab5406), rabbit anti-Gad65 (1:1,000, Millipore ab5082), rabbit anti-Gat1 (Millipore ab1570), rabbit anti-Gat3 (Millipore ab1574), rabbit anti-Maoa (1:100, Santa Cruz sc-20156), goat anti-Maob (1:50, Santa Cruz sc-18401), rabbit anti-Maob (1:100, Sigma HPA002328), mouse anti-putrescine[67] (1:50), rabbit anti-Abat (1:500, Epitomics 3359–01-01) and mouse anti-NeuN (Millipore mab377). Fluorescent secondary antibodies were purchased from Invitrogen or Jackson ImmunoResearch and used in 1:200 dilutions.

Slice immunostaining for confocal microscopy.

Sections were prepared as described above, then incubated for 1 h in a blocking solution (0.3% Triton-X, 2% normal serum in 0.1 M PBS) and then immunostained with a mixture of primary antibodies in a blocking solution at 4 °C on a shaker overnight. After washing in PBS 3 times, sections were incubated with corresponding fluorescent secondary antibodies for 3 h and then washed with PBS 3 times. If needed, DAPI staining was done by the addition of DAPI solution (Pierce, 1:1,000) during the second washing step. Finally, sections were mounted with fluorescent mounting medium (Dako) and dried. A series of fluorescent images were obtained with a FV1000 Olympus or A1 Nikon confocal microscope, and 30-μm Z stack images in 2-μm steps were processed for further analysis using FLUOVIEW (Olympus) or NIS-Elements (Nikon) software and ImageJ (NIH) program. Considering that the size of one hippocampal astrocyte is about 40 μm of diameter, 30-μm-thick Z stack images are considered to have no overlapping astrocytes along the *z* axis. Images were carefully taken to minimize over- or undersaturated pixels. Any alterations in brightness or contrast were equally applied to the entire image set. Specificity of primary antibody

and immunoreaction was confirmed by omitting primary antibodies or changing fluorescent probes of the secondary antibodies.

Immunogold electron microscopy.

For tissue fixation, the mouse, which was heterozygous for both APP/PS1 and GFAP-GFP, was deeply anesthetized and perfused with heparinized normal saline, followed by 50 ml of a freshly prepared mixture of 4% paraformaldehyde and 0.01% glutaraldehyde in 0.1 M phosphate buffer, pH 7.4 (PB). A wild-type littermate that carries only the Gfap-GFP transgene was also used for comparison with APP/PS1 mice. The hippocampi were removed and postfixed in the same fixative for 2 h at 4 °C. Sections were cut sagittally on a Vibratome at 60 μm and cryoprotected in 30% sucrose in PB overnight at 4 °C. Sections were frozen on dry ice for 20 min and then thawed in phosphate-buffered saline (PBS; 0.01 M, pH 7.2) to enhance penetration. They were pretreated with 1% sodium borohydride for 30 min to quench glutaraldehyde and then blocked with 3% H_2O_2 for 10 min to suppress endogenous peroxidases and with 10% normal donkey serum (Jackson ImmunoResearch) for 30 min to mask secondary antibody binding sites. For double immunostaining of GFP and Best1, sections of hippocampi that were pretreated as above were incubated overnight in a mixture of chicken anti-GFP (1:400, Aves labs GFP1020) and rabbit anti-Best1 (1:200, custom made) antibodies. After rinsing in PBS, sections were incubated with a mixture of biotinylated donkey anti-chicken (1:200, Jackson ImmunoResearch 703–065-155) and 1-nm gold–conjugated donkey anti-rabbit (1:50, EMS 25700) antibodies for 2–3 h. The sections were postfixed with 1% glutaraldehyde in PB for 10 min, rinsed in PBS several times, incubated for 8 min in silver intensification solution (IntenSE M, Amersham), and rinsed in 0.1 M sodium acetate and PB. They were then incubated with ExtrAvidin peroxidase (1:5,000, Sigma) for 1 h and the immunoperoxidase was visualized by nickel-intensified 3,3′-diaminobenzidine tetrahydrochloride (DAB). Sections were further rinsed in PB, osmicated (0.5% osmium tetroxide in PB) for 30 min, dehydrated in graded alcohols, flat-embedded in Durcupan ACM (Fluka) between strips of Aclar plastic film (EMS), and cured for 48 h at 60 °C. Chips containing prominent staining for GFP and Best1 in the hippocampus were cut out of the wafers and glued onto blank resin blocks with cyanoacrylate. Serially cut thin sections were collected on Formvar-coated single-slot nickel grids and stained with uranyl acetate and lead citrate. Grids were examined on a Hitachi H 7500 electron microscope (Hitachi) at 80-kV accelerating voltage. Images were captured with Digital Montage software, driving a MultiScan cooled CCD camera (ES1000W, Gatan) attached to the microscope, and saved as TIFF files. Specificity of primary antibody and immunoreaction was confirmed as described previously[9]. To control for specificity of the primary antibodies, we processed sections of DG region according to the above-described protocols, except that primary or secondary antibodies were omitted. Omission of primary or secondary antibodies completely abolished specific staining. In addition, specificity of the immunoreaction was also confirmed by the consistency of immunostaining in adjacent serial thin sections of the same astrocytes.

Image quantification.

Confocal microscopic images were analyzed using the ImageJ (NIH) program. Mean intensity values of Gfap-immunostained pixels were measured. Astrocytic GABA contents

were calculated using the mean intensity value of GABA-immunostained pixels in the GFAP staining-positive area. For that, the Gfap staining-positive area was defined by thresholding and converting into a binary mask. Pixels with sufficient Gfap fluorescence were assigned with a value of 1 and other pixels with subthreshold intensity were assigned with a value of 0. Then the Gfap-positive pixels were analyzed for GABA intensity by multiplying the GABA image times the binary mask image. The mean intensity value of pixels was used to define astrocytic GABA. The mean intensity value of interneuronal GABA-positive pixels was measured for neuronal GABA contents.

Mao enzymatic activity assay.

Mice were anesthetized and then the brain was quickly excised from the skull and submerged in ice-cold cutting solution, which is the same as the cutting solution for tonic GABA recordings. After cooling, the hippocampus was isolated, after which the CA and DG regions were separated. The fresh tissues from each mouse were homogenized, and large debris was removed by weak centrifugation. Next, the supernatant was collected and centrifuged at 13,000 r.p.m. for 20 min to obtain a mitochondria-rich fraction. The pellet was resuspended in phosphate buffer, and 20 μg were used in each well to determine the activity of the Mao. Enzymatic activity of Maoa or Maob was measured using an Amplex Red Monoamine oxidase Assay Kit (Molecular Probes) according to the manufacturer's instructions. The kit includes a 5× reaction buffer, an Amplex red reagent, horseradish peroxidase, DMSO, H_2O_2, ρ-tyramine (substrate of Maoa and Maob), benzylamine (substrate of Maob), clogyline (inhibitor of Maoa), and pargyline (inhibitor of Maob). After 2 h of enzyme reaction at 37 °C, hydrogen peroxide, which is produced by Mao activity, is measured by a color change of Amplex red reagent. The color change was quantified by measuring absorbance at 570 nm with Infinite M200 PRO microplate reader (TECAN).

Western blotting.

Western blotting was performed according to the previous report[9]. Briefly, the DG tissues were dissected from wild-type and APP/PS1 mice, and the tissues were lysed using RIPA buffer. Obtained protein lysates were separated by SDS-PAGE using 10% gels and blotted onto PVDF membranes. The blots were incubated with chicken anti-Gfap (1:2,000, Millipore ab5541) and mouse anti-Gapdh (1:5,000, Abcam ab8245). For detection of Aβ monomer and oligomers, the cytosolic fraction of DG samples were prepared as described previously[68], separated by 4–15% gels, blotted, and incubated with mouse 6E10 anti-β-amyloid peptides 1–16 (1:3,000, Covance SIG-39320–200) and mouse anti-β-actin (1:5,000, Millipore MAB1501R). Appropriate horseradish peroxidase-conjugated secondary antibodies (Jackson ImmunoResearch) were used for detection by enhanced chemiluminescence (GE Healthcare). The band intensity was acquired by ImageQuant LAS 4000 (GE Healthcare) and quantified using ImageJ software (NIH).

Quantitative real-time RT-PCR.

Quantitative real-time RT-PCR was carried out using SYBR Green PCR Master Mix as described previously[69]. In brief, reactions were performed in duplicates in a total volume of 10 μl containing 10 pM primer, 4 μl cDNA, and 5 μl power SYBR Green PCR Master

Mix (Applied Biosystems). The mRNA level of *Best1* was normalized to that of *Gapdh* mRNA. Fold-induction was calculated using the $2^{-\Delta\Delta CT}$ method[70]. The following sequences of primers were used for real-time RT-PCR. *Best1* forward: 5′-GGA TCT GGT TGT GCC TGT CT-3′; Best1 reverse: 5′ - AAG TTC TGG TGC ATC CCA TC - 3′; GAPDH forward: 5′-ACC CAG AAG ACT GTG GAT GG-3′; *Gapdh* reverse: 5′-CAC ATT GGG GGT AGG AAC AC-3′.

Passive avoidance behavioral test.

The sample sizes of mice used in the passive avoidance test were 18 for wild-type with water; 7 for wild-type with selegiline; 15 for APP/PS1 with water; 6 for APP/PS1 with selegiline. Prior to the experiment, mice were handled daily for 7 d. Mice were placed in the two-compartment (light and dark) shuttle chambers with a constant current shock generator (MED Associates). On the first experimental day, a mouse was put in the light chamber for the acquisition trial. After 60 s of exploration, the door separating the light and dark compartments was raised, allowing the mouse to freely enter the dark chamber. When the mouse entered a dark chamber with all four paws, the door immediately closed and an electric foot shock (0.5 mA, 2-s duration) was delivered through the floor grid. The mouse was then returned to the home cage and the retention trial was carried out 24 h after the acquisition trial. On the second experimental day, the mouse was placed into the light chamber again. After 60 s of exploration, the door was raised to allow the mouse enter the dark chamber. The step-through latencies of entering the dark chamber before and after the electric shock were measured to a maximum of 300 s.

Morris water maze.

The sample sizes of mice used in the Morris water maze test were 8 for wild-type with water; 4 for wild-type with selegiline; 7 for APP/PS1 with water; 4 for APP/PS1 with selegiline. Prior to the experiment, mice were handled daily for 14 d. There was no significant difference in body weight among the 4 groups tested (42.34 ± 1.52 g for wild-type with water; 38.19 ± 2.32 g for wild-type with selegiline; 41.23 ± 2.49 g for APP/PS1 with water; 40.69 ± 2.05 g for APP/PS1 with selegiline). Animals were trained to find a hidden platform (10-cm diameter) at a fixed location where the center of platform is placed 30 cm away from the wall of the pool. The water maze (1.2-m diameter) was filled with water (25 °C) and made opaque by addition of a nontoxic white paint (Weather tough Forte, Bristol Paints). The water maze was surrounded by a black circular curtain (placed 70 cm away) that held 3 salient visual cues. The releasing point was randomly distributed across 4 quadrants of the pool and the animal was allowed a maximum of 60 s to find the hidden platform. If escape did not occur within 60 s, the animal was manually guided to the platform where they stayed on for 30 s. The training consisted of 4 trials per day (10-min intertrial interval, ITI) for 14 d. On training day 9, before the training trial, animals were given 60-s probe tests (sans the platform) to test their spatial memory. On training day 15, the second probe test was performed. An automated tracking system (EthoVision, Noldus) was used to monitor the animal's swimming pattern, speed, and the amount of time spent in each of the four quadrants. The experimenter was blinded to the genotype or treatment during Morris water maze experiment.

Human brain samples.

Neuropathological processing of control and AD human brain samples followed the procedures previously established for the Boston University Alzheimer's Disease Center (BUADC). Temporal cortical regions were used for experiments. Institutional Review Board approval for ethical permission was obtained through the BUADC. Next of kin provided informed consent for participation and brain donation. The study was performed in accordance with principles of human subject protection in the Declaration of Helsinki. Detailed information of brain tissues is described in Supplementary Table 3. In all cases where AD was diagnosed at autopsy, AD was stated as the cause of death.

Real-time PCR from human samples.

RNA was isolated by NucleoSpin Total RNA isolation kit (Macherey-Nagel), and cDNA was generated using Maxime RT PreMix Oligo dT primer kit (Intron biotechnology). Real-time PCR was performed on the cDNA samples using an ABI Stepone 2.1 (Applied Biosystems). Specific primers for human *GFAP* (Forward: CTT TGC CAG CTA CAT CGA GA, Reverse: ATT GTC CCT CTC AAC CTC CA) and human *MAOB* (Forward: CCC ACC TGT ATG GAA TCC A, Reverse: CAG TGA CAC ACA GGT TCA CA) were used. Human *GAPDH* (Forward: ACA GCC GCA TCT TCT TGT GCA GTG, Reverse: GGC CTT GAC TGT GCC GTT GAA TTT) was used as endogenous control to standardize the amount of RNA in each reaction.

Stab wound injury.

Mice were deeply anesthetized with 2% avertin (20 μg g^{-1}, i.p.) and mounted in a stereotaxic frame (Kopf). The scalp was incised and a hole drilled into the skull above the hippocampus (AP, –1.8 mm; ML, –1 mm from bregma)[61]. A 0.4-mm-diameter spring steel pin (BioQuip) was slowly introduced into the hippocampus until the tip was located at –2 mm below the dura, left for 3 min and then slowly retracted. 5 d after surgery, mice were killed for immunostaining and confocal microscopy.

Statistical analyses.

When two groups were being compared, the significance of data was assessed by the two-tailed Student's unpaired *t*-test using Microsoft Excel software. For comparison of multiple groups, two-way analysis of variance (ANOVA), repeated-measures two-way ANOVA, repeated-measures one-way ANOVA and one-way ANOVA with Scheffe's *post hoc* analysis were assessed using SPSS 20 (IBM) software. Homogeneity of variance was tested using F test. In the case of repeated measures, sphericity was tested using Mauchly's test. P values less than 0.05 were considered significant. The significance level is displayed as asterisks ($*P < 0.05$, $**P < 0.01$, $***P < 0.001$; NS, not significant). For all comparisons, samples were not excluded from data except only for tonic GABA current recording; cells with holding current over –100 pA were excluded, and experiments were stopped after 3 h from the time of slicing. No animal was excluded from analysis in behavioral experiments. Detailed results for ANOVA are described in Supplementary Table 2. No statistical method was used to predetermine sample size. The experiments were not randomized.

Supplementary Material

Refer to Web version on PubMed Central for supplementary material.

ACKNOWLEDGMENTS

This work was supported by the WCI Program of the National Research Foundation of Korea (NRF) funded by the Ministry of Science, ICT and Future Planning (MSIP: to C.J.L., NRF grant number: WCI 2009–003), the KIST Institutional Flagship Program (to C.J.L., 3E25022; to H.R., 2E24380), the National Leading Research Laboratory Program of Korea and the KAIST Future Systems Healthcare Project (to D.K., NRF grant number: 2011–0028772), the Basic Science Research Program through the NRF funded by the MSIP (to Y.C.B., 2008–0062282), and the National Institute of Aging of USA (to N.W.K.). We thank Mazence for APP/PS1 mice, W. Park (GIST) for 5XFAD mice, K. Park and H. Song (KIST) for safinamide and K. Fujiwara (Sojo University) for the putrescine-specific antibody.

References

1. Alzheimer's Association. 2012 Alzheimer's disease facts and figures.Alzheimers Dement8, 131–168 (2012). [PubMed: 22404854]
2. Mattson MP. Pathways towards and away from Alzheimer's disease.Nature430, 631–639 (2004). [PubMed: 15295589]
3. Mucke L & Selkoe DJ. Neurotoxicity of amyloid β-protein: synaptic and network dysfunction. Cold Spring Harb. Perspect. Med 2, a006338 (2012). [PubMed: 22762015]
4. Ballatore C, Lee VM-Y & Trojanowski JQ. Tau-mediated neurodegeneration in Alzheimer's disease and related disorders. Nat. Rev. Neurosci 8, 663–672 (2007). [PubMed: 17684513]
5. Eddleston M & Mucke L. Molecular profile of reactive astrocytes—implications for their role in neurologic disease. Neuroscience 54, 15–36 (1993). [PubMed: 8515840]
6. Wisniewski HM & Wegiel J. Spatial relationships between astrocytes and classical plaque components. Neurobiol. Aging 12, 593–600 (1991). [PubMed: 1770990]
7. Sofroniew MV. Molecular dissection of reactive astrogliosis and glial scar formation.Trends Neurosci32, 638–647 (2009). [PubMed: 19782411]
8. Kuchibhotla KV, Lattarulo CR, Hyman BT & Bacskai BJ. Synchronous hyperactivity and intercellular calcium waves in astrocytes in Alzheimer mice. Science 323, 1211–1215 (2009). [PubMed: 19251629]
9. Woo DHet al.TREK-1 and Best1 channels mediate fast and slow glutamate release in astrocytes upon GPCR activation.Cell151, 25–40 (2012). [PubMed: 23021213]
10. Henneberger C, Papouin T, Oliet SH & Rusakov DA. Long-term potentiation depends on release of d-serine from astrocytes. Nature 463, 232–236 (2010). [PubMed: 20075918]
11. Blum AE, Joseph SM, Przybylski RJ & Dubyak GR. Rho-family GTPases modulate Ca^{2+}-dependent ATP release from astrocytes. Am. J. Physiol. Cell Physiol 295, C231–C241 (2008). [PubMed: 18495810]
12. Lee Set al.Channel-mediated tonic GABA release from glia.Science330, 790–796 (2010). [PubMed: 20929730]
13. Farrant M & Nusser Z. Variations on an inhibitory theme: phasic and tonic activation of $GABA_A$ receptors. Nat. Rev. Neurosci 6, 215–229 (2005). [PubMed: 15738957]
14. Samakashvili Set al.Analysis of chiral amino acids in cerebrospinal fluid samples linked to different stages of Alzheimer disease.Electrophoresis32, 2757–2764 (2011). [PubMed: 21983823]
15. Yoshiike Yet al.$GABA_A$ Receptor-mediated acceleration of aging-associated memory decline in APP/PS1 mice and its pharmacological treatment by picrotoxin.PLoS ONE3, e3029 (2008). [PubMed: 18716656]
16. Yoon BEet al.The amount of astrocytic GABA positively correlates with the degree of tonic inhibition in hippocampal CA1 and cerebellum.Mol. Brain4, 42 (2011). [PubMed: 22107761]

17. Borchelt DRet al.Accelerated amyloid deposition in the brains of transgenic mice coexpressing mutant presenilin 1 and amyloid precursor proteins.Neuron19, 939–945 (1997). [PubMed: 9354339]
18. Kamphuis Wet al.GFAP isoforms in adult mouse brain with a focus on neurogenic astrocytes and reactive astrogliosis in mouse models of Alzheimer disease.PLoS ONE7, e42823 (2012). [PubMed: 22912745]
19. Volianskis A, Køstner R, Mølgaard M, Hass S & Jensen MS. Episodic memory deficits are not related to altered glutamatergic synaptic transmission and plasticity in the CA1 hippocampus of the APPswe/PS1ΔE9-deleted transgenic mice model of β-amyloidosis. Neurobiol. Aging 31, 1173–1187 (2010). [PubMed: 18790549]
20. Irizarry MCet al.Aβ deposition is associated with neuropil changes, but not with overt neuronal loss in the human amyloid precursor protein V717F (PDAPP) transgenic mouse.J. Neurosci17, 7053–7059 (1997). [PubMed: 9278541]
21. Matousek SBet al.Chronic IL-1β–mediated neuroinflammation mitigates amyloid pathology in a mouse model of Alzheimer's disease without inducing overt neurodegeneration.J. Neuroimmune Pharmacol7, 156–164 (2012). [PubMed: 22173340]
22. Hartlage-Rübsamen Met al.Glutaminyl cyclase contributes to the formation of focal and diffuse pyroglutamate (pGlu)-Aβ deposits in hippocampus via distinct cellular mechanisms.Acta Neuropathol121, 705–719 (2011). [PubMed: 21301857]
23. Kesner RP. A behavioral analysis of dentate gyrus function.Prog. Brain Res163, 567–576 (2007). [PubMed: 17765738]
24. Nakashiba Tet al.Young dentate granule cells mediate pattern separation, whereas old granule cells facilitate pattern completion.Cell149, 188–201 (2012). [PubMed: 22365813]
25. Cao D, Lu H, Lewis TL & Li L. Intake of sucrose-sweetened water induces insulin resistance and exacerbates memory deficits and amyloidosis in a transgenic mouse model of Alzheimer disease. J. Biol. Chem 282, 36275–36282 (2007). [PubMed: 17942401]
26. Han K-Set al.Channel-mediated astrocytic glutamate release via Bestrophin-1 targets synaptic NMDARs.Mol. Brain6, 4 (2013). [PubMed: 23324492]
27. Park Het al.High glutamate permeability and distal localization of Best1 channel in CA1 hippocampal astrocyte.Mol. Brain6, 54 (2013). [PubMed: 24321245]
28. Seiler N, Sshmidt-Glenewinkel T & Sarhan S. On the formation of γ-aminobutyric acid from putrescine in brain. J. Biochem 86, 277–279 (1979). [PubMed: 479128]
29. Laschet J, Grisar T, Bureau M & Guillaume D. Characteristics of putrescine uptake and subsequent GABA formation in primary cultured astrocytes from normal C57BL/6J and epileptic DBA/2J mouse brain cortices. Neuroscience 48, 151–157 (1992). [PubMed: 1584419]
30. Caspi Ret al.The MetaCyc database of metabolic pathways and enzymes and the BioCyc collection of pathway/genome databases.Nucleic Acids Res40, D742–D753 (2012). [PubMed: 22102576]
31. Seiler N & Al-Therib M. Putrescine catabolism in mammalian brain. Biochem. J 144, 29–35 (1974). [PubMed: 4156831]
32. Saura Jet al.Increased monoamine oxidase B activity in plaque-associated astrocytes of Alzheimer brains revealed by quantitative enzyme radioautography.Neuroscience62, 15–30 (1994). [PubMed: 7816197]
33. Nakamura Set al.Expression of monoamine oxidase B activity in astrocytes of senile plaques.Acta Neuropathol80, 419–425 (1990). [PubMed: 2239154]
34. Saura J, Kettler R, Da Prada M & Richards J. Quantitative enzyme radioautography with 3H-Ro 41–1049 and 3H-Ro 19–6327 in vitro: localization and abundance of MAO-A and MAO-B in rat CNS, peripheral organs, and human brain. J. Neurosci 12, 1977–1999 (1992). [PubMed: 1578281]
35. Levitt P, Pintar JE & Breakefield XO. Immunocytochemical demonstration of monoamine oxidase B in brain astrocytes and serotonergic neurons. Proc. Natl. Acad. Sci. USA 79, 6385–6389 (1982). [PubMed: 6755469]
36. Birkmayer W, Riederer P, Youdim M & Linauer W. The potentiation of the anti akinetic effect after l-dopa treatment by an inhibitor of MAO-B, Deprenil. J. Neural Transm 36, 303–326 (1975). [PubMed: 1172524]

37. Youdim MBet al.Rasagiline: neurodegeneration, neuroprotection, and mitochondrial permeability transition.J. Neurosci. Res79, 172–179 (2005). [PubMed: 15573406]
38. Nägga K, Bogdanovic N & Marcusson J. GABA transporters (GAT-1) in Alzheimer's disease. J. Neural Transm 106, 1141–1149 (1999). [PubMed: 10651110]
39. Lee J, Kannagi M, Ferrante RJ, Kowall NW & Ryu H. Activation of Ets-2 by oxidative stress induces Bcl-xL expression and accounts for glial survival in amyotrophic lateral sclerosis. FASEB J 23, 1739–1749 (2009). [PubMed: 19179380]
40. Turrigiano GG. The self-tuning neuron: synaptic scaling of excitatory synapses.Cell135, 422–435 (2008). [PubMed: 18984155]
41. Allen C & Stevens CF. An evaluation of causes for unreliability of synaptic transmission. Proc. Natl. Acad. Sci. USA 91, 10380–10383 (1994). [PubMed: 7937958]
42. Gimbel DAet al.Memory impairment in transgenic Alzheimer mice requires cellular prion protein.J. Neurosci30, 6367–6374 (2010). [PubMed: 20445063]
43. De Angelis L & Furlan C. The anxiolytic-like properties of two selective MAOIs, moclobemide and selegiline, in a standard and an enhanced light/dark aversion test. Pharmacol. Biochem. Behav 65, 649–653 (2000). [PubMed: 10764917]
44. Wilcock GK, Birks J, Whitehead A & Evans SJ. The effect of selegiline in the treatment of people with Alzheimer's disease: a meta-analysis of published trials. Int. J. Geriatr. Psychiatry 17, 175–183 (2002). [PubMed: 11813282]
45. Engberg G, Elebring T & Nissbrandt H. Deprenyl (selegiline), a selective MAO-B inhibitor with active metabolites; effects on locomotor activity, dopaminergic neurotransmission and firing rate of nigral dopamine neurons. J. Pharmacol. Exp. Ther 259, 841–847 (1991). [PubMed: 1658311]
46. Marzo Aet al.Pharmacokinetics and pharmacodynamics of safinamide, a neuroprotectant with antiparkinsonian and anticonvulsant activity.Pharmacol. Res50, 77–85 (2004). [PubMed: 15082032]
47. Squire LR, Stark CE & Clark RE. The medial temporal lobe*. Annu. Rev. Neurosci 27, 279–306 (2004). [PubMed: 15217334]
48. Palop JJ, Chin J & Mucke L. A network dysfunction perspective on neurodegenerative diseases. Nature 443, 768–773 (2006). [PubMed: 17051202]
49. Pike CJ, Cummings B, Monzavi R & Cotman CW. β-amyloid–induced changes in cultured astrocytes parallel reactive astrocytosis associated with senile plaques in Alzheimer's disease. Neuroscience 63, 517–531 (1994). [PubMed: 7891862]
50. Chen Get al.A learning deficit related to age and β-amyloid plaques in a mouse model of Alzheimer's disease.Nature408, 975–979 (2000). [PubMed: 11140684]
51. Hsieh Het al.AMPAR removal underlies Aβ-induced synaptic depression and dendritic spine loss.Neuron52, 831–843 (2006). [PubMed: 17145504]
52. Scheff SW & Price DA. Synaptic density in the inner molecular layer of the hippocampal dentate gyrus in Alzheimer disease. J. Neuropathol. Exp. Neurol 57, 1146–1153 (1998). [PubMed: 9862637]
53. Jacobs K, Kharazia VN & Prince DA. Mechanisms underlying epileptogenesis in cortical malformations. Epilepsy Res 36, 165–188 (1999). [PubMed: 10515164]
54. Verret Let al.Inhibitory interneuron deficit links altered network activity and cognitive dysfunction in Alzheimer model.Cell149, 708–721 (2012). [PubMed: 22541439]
55. Piccinin GL, Finali G & Piccirilli M. Neuropsychological effects of l-deprenyl in Alzheimer's type dementia. Clin. Neuropharmacol 13, 147–163 (1990). [PubMed: 2109658]
56. Tariot PNet al.l-deprenyl in Alzheimer's disease: preliminary evidence for behavioral change with monoamine oxidase B inhibition.Arch. Gen. Psychiatry44, 427–433 (1987). [PubMed: 3107514]
57. Monteverde A, Gnemmi P, Rossi F & Finali G. Selegiline in the treatment of mild to moderate Alzheimer-type dementia. Clin. Ther 12, 315–322 (1990). [PubMed: 2121360]
58. Birks J & Flicker L. Selegiline for Alzheimer's disease. Cochrane Database Syst. Rev CD000442 (2003). [PubMed: 12535396]
59. Gerlach M, Youdim M & Riederer P. Pharmacology of selegiline. Neurology 47, S137–S145 (1996). [PubMed: 8959982]

60. Barres BA. The mystery and magic of glia: a perspective on their roles in health and disease.Neuron60, 430–440 (2008). [PubMed: 18995817]

61. Paxinos G & Franklin K The Mouse Brain in Stereotaxic Coordinates: Compact Second Edition (Academic Press, San Diego, 2003).

62. Kutlán D & Molnar-Perl I. New aspects of the simultaneous analysis of amino acids and amines as their o-phthaldialdehyde derivatives by high-performance liquid chromatography. Analysis of wine, beer and vinegar. J. Chromatogr. A 987, 311–322 (2003). [PubMed: 12613825]

63. Mengerink Y, Kutlan D, Toth F, Csampai A & Molnar-Perl I. Advances in the evaluation of the stability and characteristics of the amino acid and amine derivatives obtained with the o-phthaldialdehyde/3-mercaptopropionic acid and o-phthaldialdehyde/N-acetyl-l-cysteine reagents. High-performance liquid chromatography-mass spectrometry study. J. Chromatogr. A 949, 99–124 (2002). [PubMed: 11999763]

64. Kim YS, Moss JA & Janda KD. Biological tuning of synthetic tactics in solid-phase synthesis: Application to Aβ (1–42). J. Org. Chem 69, 7776–7778 (2004). [PubMed: 15498016]

65. Unal Cevik I & Dalkara T. Intravenously administered propidium iodide labels necrotic cells in the intact mouse brain after injury. Cell Death Differ 10, 928–929 (2003). [PubMed: 12868000]

66. Park Het al.Bestrophin-1 encodes for the Ca^{2+}-activated anion channel in hippocampal astrocytes.J. Neurosci29, 13063–13073 (2009). [PubMed: 19828819]

67. Fujiwara K, Tanabe T, Yabuuchi M, Ueoka R & Tsuru D. A monoclonal antibody against the glutaraldehyde-conjugated polyamine, putrescine: application to immunocytochemistry. Histochem. Cell Biol 115, 471–477 (2001). [PubMed: 11455447]

68. Sehgal Net al.Withania somnifera reverses Alzheimer's disease pathology by enhancing low-density lipoprotein receptor-related protein in liver.Proc. Natl. Acad. Sci. USA109, 3510–3515 (2012). [PubMed: 22308347]

69. Hong Jet al.Microglial Toll-like receptor 2 contributes to kainic acid-induced glial activation and hippocampal neuronal cell death.J. Biol. Chem285, 39447–39457 (2010). [PubMed: 20923777]

70. Livak KJ & Schmittgen TD. Analysis of relative gene expression data using real-time quantitative PCR and the $2^{-\Delta\Delta CT}$ method. Methods 25, 402–408 (2001). [PubMed: 11846609]

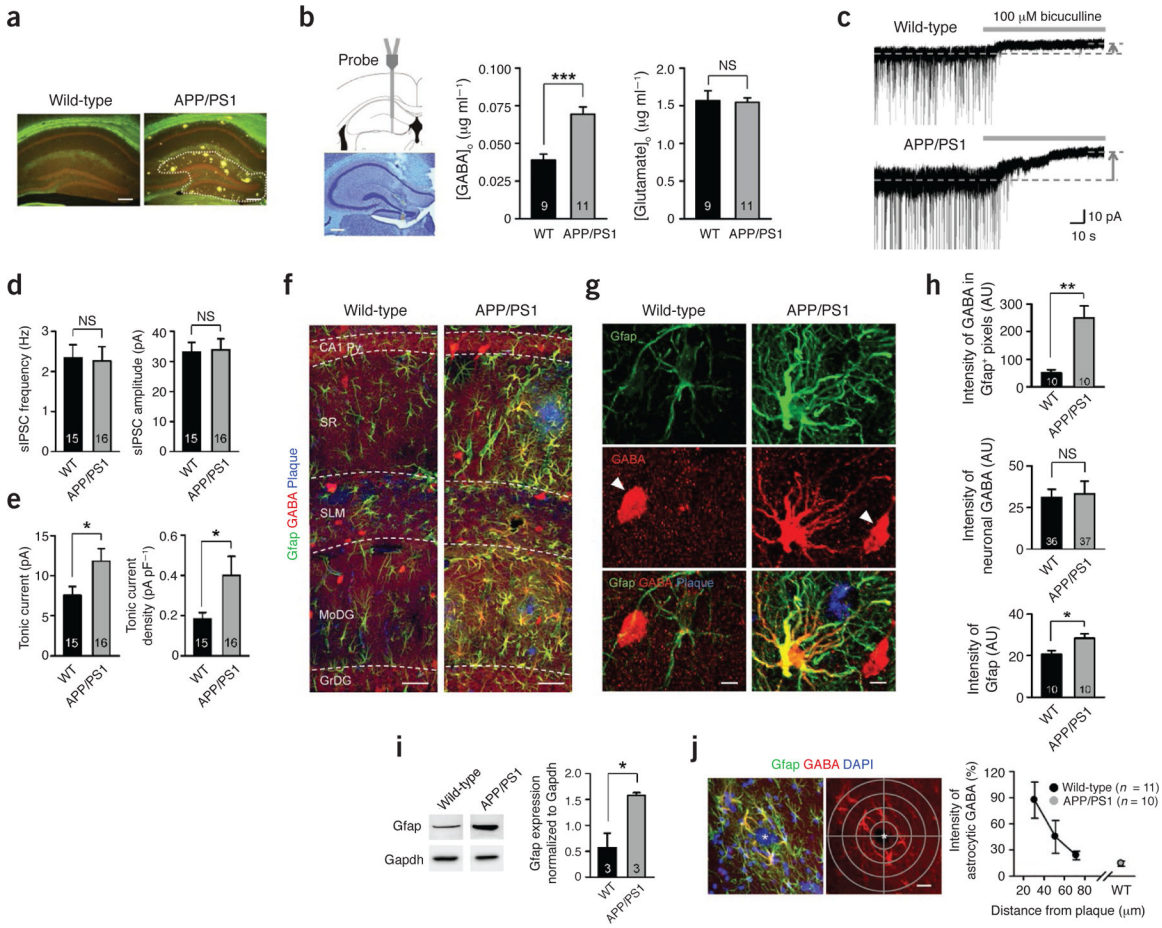

Figure 1.

Increased tonic GABA release and GABA immunoreactivity in reactive astrocytes. (**a**) Thioflavin-S staining of amyloid plaques (yellowish green) in the hippocampus. Dotted line indicates DG ($n \geq 10$ for each group; males at 10 months of age; scale bar, 200 μm). (**b**) *In vivo* microdialysis (males at 10–11 months of age). Left, validation of microdialyzed sites by cresyl violet staining (scale bar, 200 μm). Middle, GABA levels in dialysate measured by HPLC. ***$P < 0.001$ (Student's *t*-test). Right, glutamate levels. NS, $P > 0.05$ (Student's *t*-test). $[GABA]_o$ or $[Glutamate]_o$, the concentrations of GABA or glutamate in outer space of cells. WT, wild type. (**c**) Representative trace of $GABA_A$ receptor–mediated current recorded from granule cells of the DG ($n = 4$ for WT; $n = 7$ for APP/PS1; both sexes at 8.5–13 months of age). Dashed lines and arrows indicate baseline shift with bicuculline (100 μM) application (gray bar). (**d**) Left, frequency of sIPSCs before bicuculline application. Right, amplitude of sIPSCs before bicuculline application. (**e**) Left, amplitude of tonic GABA current. *$P < 0.05$ (Student's *t*-test). Right, density of tonic GABA current measured by dividing current amplitude by membrane capacitance. *$P < 0.05$ (Student's *t*-test). (**f**–**h**) Immunostaining and quantification of images taken from the molecular layer of DG ($n = 5$ for each group; both sexes at 8–11 months of age). (**f**) Representative confocal images of Gfap-, GABA- and thioflavin-S–stained plaques (scale bar, 20 μm). SR, striatum radiatum; SLM, striatum lacunosum moleculare; Py, pyramidal neuron layer; MoDG, molecular layer of dentate gyrus; GrDG, granule cell layer of dentate gyrus. (**g**) High-magnification images

of an astrocyte. Arrowheads indicate GABAergic neurons (scale bar, 5 μm). (**h**) Top, mean intensity of GABA in GFAP-positive areas. $^{**}P < 0.01$, $^{*}P < 0.05$ (Student's *t*-test). AU, arbitrary units. Middle, mean intensity of interneuronal GABA. Bottom, mean intensity of Gfap. (**i**) Left, representative western blots of Gfap in the DG ($n = 3$ for each group; both sexes at 11–11.5 months of age). Right, quantification of Gfap by densitometry. $^{*}P < 0.05$ (Student's *t*-test). (**j**) Left, a graticule with 20-μm density (gray) focused at the center of plaque (asterisks) was applied to confocal images (scale bar, 20 μm). Right, normalized intensity of astrocytic GABA according to the distance from the center of a plaque. 0% indicates background intensity, and 100% indicates the mean intensity of neuronal GABA in the same confocal image. Number on each bar refers to the number of mice (**b**,**i**), slices (**d**), images (**h** top and bottom, **j**), and cells (**h** middle) analyzed. *n* refers to the number of animals studied. Data are means ± s.e.m.

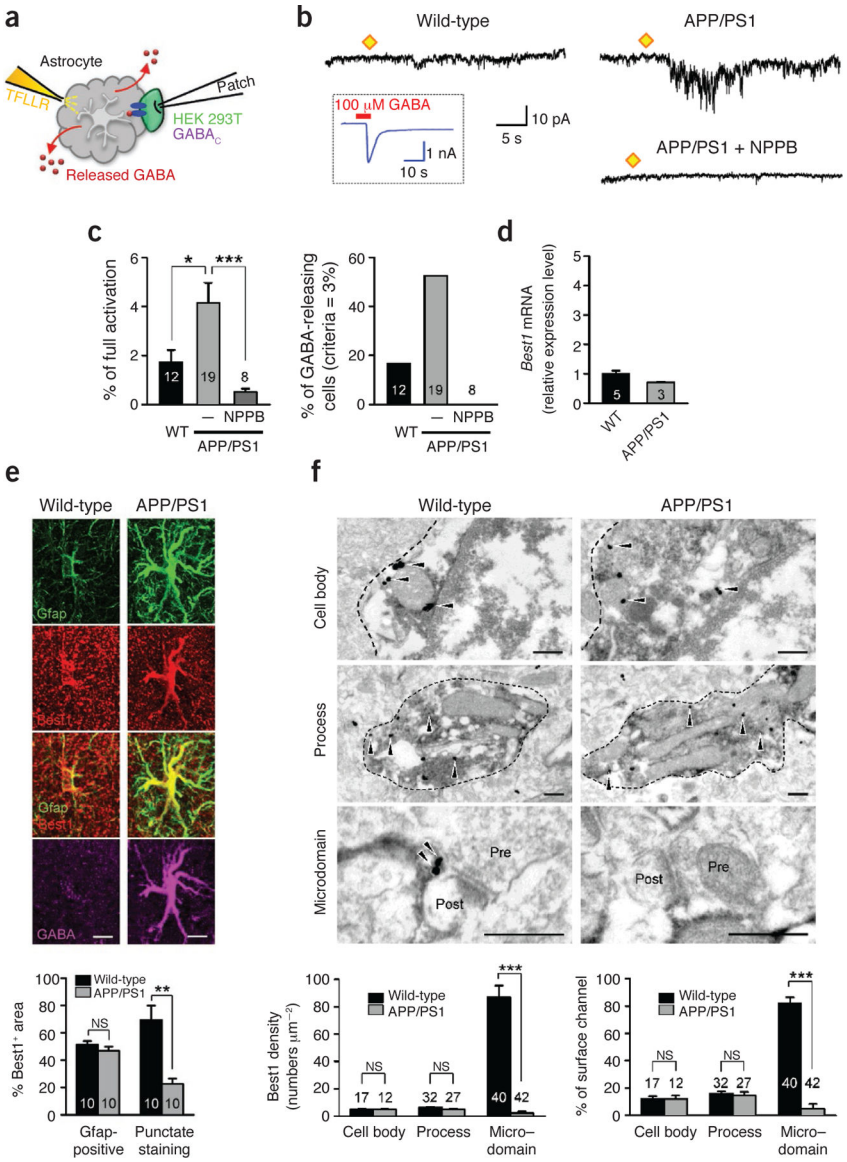

Figure 2.

GABA is released from reactive astrocytes via redistributed Best1 channel. (**a**) Schematic diagram of sniffer-patch technique. Left pipette (yellow): pressure application of TFLLR to astrocyte (gray). Right pipette: recording pipette for HEK 293T cell expressing $GABA_C$ (green, sensor cell). (**b**) Representative trace of sensor current recorded in HEK 293T cell and induced by GABA from an astrocyte of wild-type, APP/PS1 and APP/PS1 with NPPB treatment (50 μM). Diamonds, TFLLR puffing (500 μM, 100 ms, 10 pounds per square inch (p.s.i.)). Inset, full activation of sensor by applying GABA (100 μM, red bar). (**c**) Left, peak amplitude of $GABA_C$ current normalized to full activation. $*P < 0.05$, $***P < 0.001$ (Student's *t*-test). Right, percentage of GABA-releasing astrocytes of which peak amplitude measured by sensor cell is higher than 3% of full activation. For **b** and **c**, $n = 2$ for WT; $n = 4$ for APP/PS1; $n = 2$ for APP/PS1 + NPPB; males at 8–18 months of age. (**d**) Quantitative real-time PCR ($n = 5$ for wild-type; $n = 3$ for APP/PS1; both sexes at 11–11.5

months of age). Relative expression level of *Best1* mRNA in DG. (**e**) Immunostaining and quantification of Best1 in the molecular layer of DG (both sexes at 9 months of age; scale bar, 10 μm). Top, representative confocal images of an astrocyte. Bottom, percentage of Best1-positive areas in cell body and process or in microdomain over total area. $^{**}P < 0.01$ (Student's *t*-test). (**f**) Immunogold electron microscopy of Best1 in the molecular layer of DG (males at 12 months of age). Top, representative images of Best1 labeling (black dots indicated by arrowheads) in DAB-stained astrocytes (outlined with dashed lines). Pre, presynaptic terminal; Post, postsynapse; scale bar, 300 nm. Bottom left, density of gold particles for Best1 in cell body, process and microdomain. $^{***}P < 0.001$ (Student's *t*-test). Bottom right, percentage of gold particles for Best1 located on the plasma membrane of cell body, process and microdomain. $^{***}P < 0.001$ (Student's *t*-test). Number on each bar refers to the number of cells (**c**,**e**), mice (**d**) or images (**f**) analyzed. *n* refers to the number of animals studied. Data are means ± s.e.m.

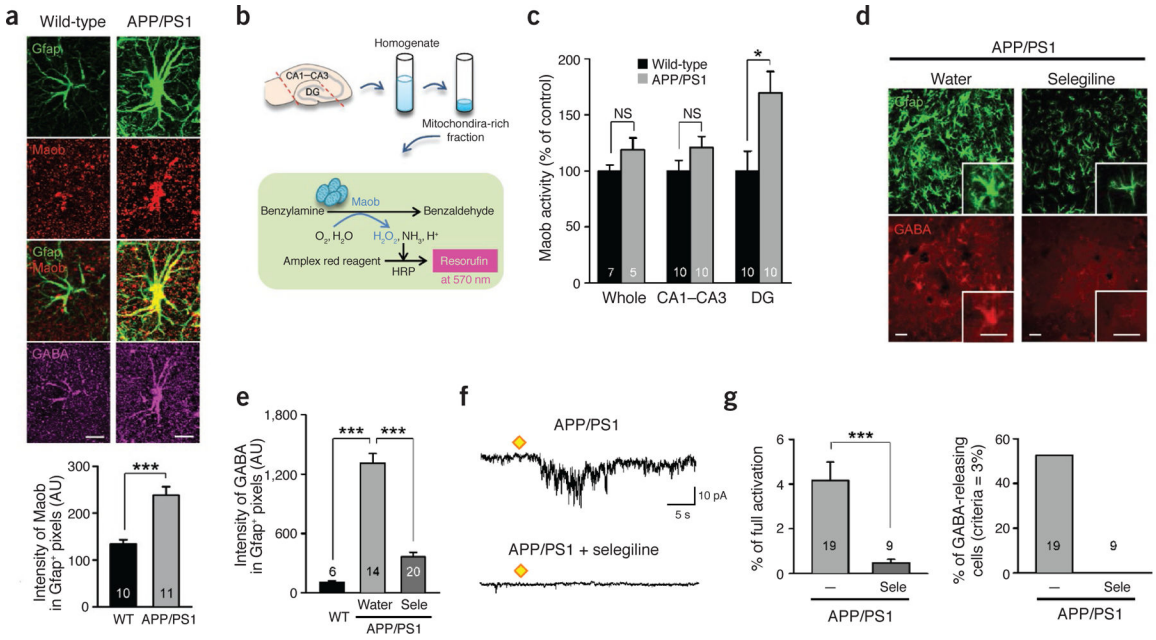

Figure 3.

Maob is responsible for GABA production in reactive astrocytes. (**a**) Immunostaining and quantification of Maob in the molecular layer of DG (females at 10 months of age). Top, representative confocal images of an astrocyte (scale bar, 10 μm). Bottom, mean intensity of Maob in Gfap-positive areas. ***$P < 0.001$ (Student's *t*-test). (**b**) Reaction diagram of the enzyme activity assay of Maob in the hippocampus. (**c**) Maob activity normalized to the activity of wild-type mice in the whole hippocampus or subregions ($n = 7$ for wild-type whole; $n = 5$ for other groups; For CA1–CA3 and DG groups, left and right hippocampus were analyzed separately; males at 12 months of age). *$P < 0.05$ (Student's *t*-test). (**d**,**e**) Immunostaining and quantification of astrocytic GABA after oral administration of selegiline (Sele; 10 mg kg^{-1} d^{-1} for 3 d) in APP/PS1 mice ($n = 1$ for wild-type; $n = 3$ for APP/PS1 with water; $n = 4$ for APP/PS1 with Sele; males at 12 months of age). (**d**) Representative confocal images of Gfap and GABA in the molecular layer of DG. Inset, magnified images. Scale bars, 30 μm for both main images and the insets. (**e**) Mean intensity of GABA in Gfap-positive areas. ***$P < 0.001$ (Student's *t*-test). (**f**,**g**) Measurement of GABA release from acutely dissociated hippocampal astrocytes ($n = 4$ for APP/PS1; $n = 1$ for APP/PS1 + selegiline; males at 8–18 months of age). (**f**) Representative trace of sensor current induced by GABA from an astrocyte of an APP/PS1 mouse and an astrocyte from an APP/PS1 mouse with selegiline treatment (100 nM). Diamonds, TFLLR puffing (500 μM, 100 ms, 10 p.s.i.). The APP/PS1 group is the same group from Figure 2b. (**g**) Left, peak amplitude of $GABA_C$ current normalized to full activation. ***$P < 0.001$ (Student's *t*-test). Right, percentage of GABA-releasing astrocytes of which peak amplitude measured by sensor cell is higher than 3% of full activation. The APP/PS1 group is the same group from Figure 2c. Number on each bar refers to the number of hippocampi (**c**), images (**e**) or cells (**a**,**g**) analyzed. *n* refers to the number of animals studied. Data are means ± s.e.m.

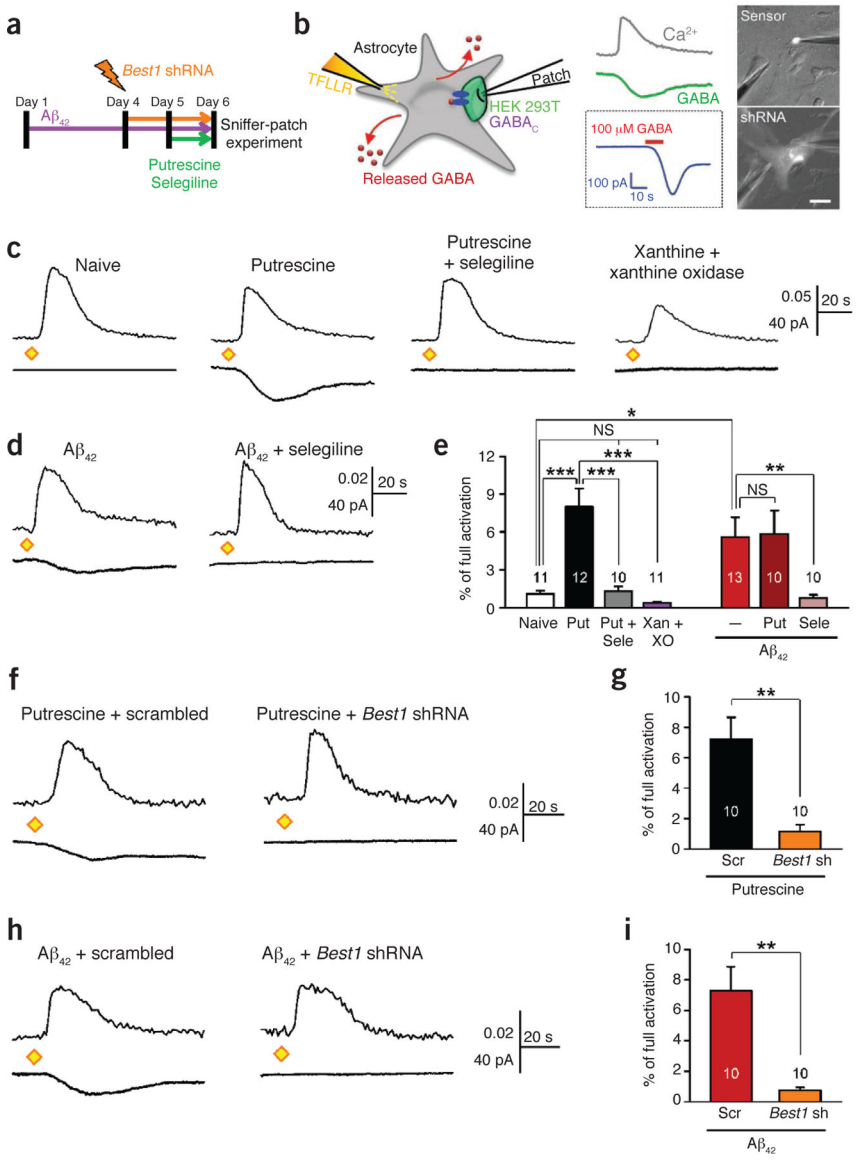

Figure 4.

Maob-mediated production and Best1-mediated release of GABA in cultured hippocampal astrocytes. (**a**) Experimental protocol for sniffer-patch technique with cultured astrocytes. Putrescine (180 μM) and selegiline (100 nM) were present in culture medium overnight. $A\beta_{42}$ (10 μM) was present in culture medium for 5 d. For *Best1* knockdown experiments, *Best1* shRNA or scrambled shRNA was transfected into astrocytes by electroporation. (**b**) Left, schematic diagram of sniffer-patch technique. Middle, representative traces recorded. Ca^{2+} transient recorded from Fura-2–loaded astrocyte (gray trace), whole-cell current recorded from $GABA_C$-expressing sensor cell upon TFLLR pressure application (green trace), and full activation of sensor (blue trace) by applying GABA (100 μM, red bar). Right, fluorescence images for sniffer patch (scale bar, 50 μm). A sensor cell expresses GFP (top), and an astrocyte transfected with shRNA expresses mCherry (bottom). Data are representative of >100 recordings and 10 experiments. (**c**,**d**) Representative traces of sensor

current induced by GABA from cultured astrocytes treated in naive conditions or with putrescine, putrescine and selegiline, or xanthine (50 μM) and xanthine oxidase (5 mU ml^{-1}) (**c**) or with $A\beta_{42}$ or $A\beta_{42}$ and selegiline (**d**). Diamonds, TFLLR puffing (500 μM, 100 ms, 10 p.s.i.). Data are representative of ≥10 recordings and 2 or 3 experiments. (**e**) Peak amplitude of sensor current normalized to full activation. $*P < 0.05$, $**P < 0.01$ (Student's *t*-test). $***P < 0.001$ (one-way analysis of variance (ANOVA) and Sheffe's test). XO, xanthine oxidase. (**f**) Representative trace of sensor current induced by GABA from putrescine-treated astrocytes transfected with scrambled shRNA or *Best1* shRNA. Data are representative of ≥10 recordings and 2 experiments. (**g**) Peak amplitude of $GABA_C$ current normalized to full activation. $**P < 0.01$ (Student's *t*-test). (**h**) Representative trace of sensor current induced by GABA from $A\beta_{42}$-treated astrocytes transfected with scrambled shRNA or *Best1* shRNA. Data are representative of ≥10 recordings and 2 experiments. (**i**) Peak amplitude of $GABA_C$ current normalized to full activation. $**P < 0.01$ (Student's *t*-test). Number on each bar refers to the number of cells recorded. Each cell was recorded once. $n = 3$ for Naive; $n = 4$ for Put; $n = 1$ for Put + Sele; $n = 1$ for Xan + XO; $n = 4$ for $A\beta_{42}$; $n = 3$ for $A\beta_{42}$ + Put; $n = 2$ for $A\beta_{42}$ + Sele for **e** and $n = 2$ for each group in **g**,**i**. *n* indicates the number of animals tested. Data are means ± s.e.m.

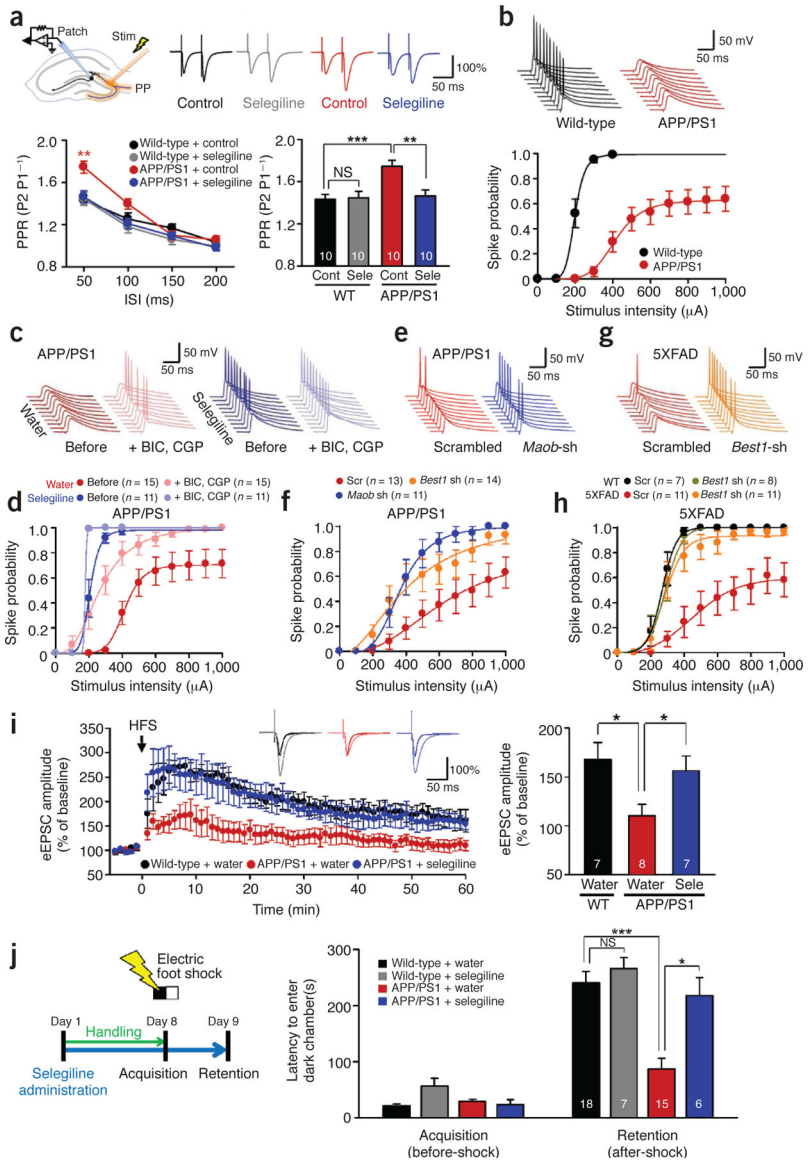

Figure 5.

Impaired presynaptic release probability, spike probability, synaptic plasticity, and learning and memory are fully rescued by targeting *Maob* or *Best1*. (**a**) PPR of eEPSCs recorded from dentate granule cells in wild-type and APP/PS1 mice with or without pretreatment with selegiline (100 μM) ($n = 2$ for each group; both sexes at 12–12.5 months of age). Top left, schematic diagram for input-output relationship, PPR, spike probability and LTP experiments in granule cells of DG. Stim, electrical stimulation; PP, perforant path. Top right, representative traces of eEPSCs evoked by paired-pulse stimuli at 300-μA intensity and 50-ms interpulse interval. Data are representative of >10 recordings and 2 experiments. Bottom left, PPR of eEPSCs plotted as a function of interspike intervals (ISIs). $P < 0.05$ for drug (two-way repeated-measures ANOVA); $^{**}P < 0.01$ for APP/PS1 + control at 50 ms (one-way ANOVA and Bonferroni's test). Bottom right, mean PPR measured at 50-ms interspike interval. $^{**}P < 0.01$, $^{***}P < 0.001$ (two-way ANOVA and Bonferroni's test). (**b**)

Evoked spike probability by electrical stimulation of perforant path (0.1 Hz, 100 μs, 100–1,000 μA) (n = 3 for each group; both sexes at 12–13 months of age). Top, representative traces of evoked EPSPs and action potentials at 300-μA stimulation. Bottom, summary graph of spike probability versus stimulus intensity. (**c**) Representative trace of evoked EPSPs in the DG granule cells of APP/PS1 mice treated with GABA receptor antagonists (BIC: 10 μM bicuculline, CGP: 5 μM CGP55845) and the Maob inhibitor selegiline (10 mg kg^{-1} d^{-1} oral administration for 7 d) at 300-μA stimulation (n = 3 for water; n = 2 for selegiline; both sexes at 12–13 months of age). Experiments were repeated more than twice. (**d**) Summary graph of spike probability of granule cells recorded in Figure 5c versus stimulus intensity. (**e**) Representative traces of evoked EPSPs in the DG granule cells of APP/PS1 mice injected with scrambled, *Best1* or *Maob* shRNA at 400-mA stimulation (n = 3 for scrambled; n = 2 for *Best1* shRNA; n = 2 for *Maob* shRNA; both sexes at 10–11 months of age). Experiments were repeated more than twice. (**f**) Summary graph of spike probability of granule cells recorded in Figure 5e versus stimulus intensity. (**g**) Representative traces of evoked EPSPs in the DG granule cells of 5XFAD mice injected with scrambled or *Best1* shRNA at 400-mA stimulation (n = 2 for WT scrambled; n = 2 for WT *Best1* shRNA; n = 3 for 5XFAD scrambled; n = 3 for 5XFAD *Best1* shRNA; males at 7–8 months of age). (**h**) Summary graph of spike probability of granule cells recorded in Figure 5g versus stimulus intensity. (**i**) LTP recorded from dentate granule cells of wild-type and APP/PS1 mice with or without oral administration of selegiline (10 mg kg^{-1} d^{-1} for 7 d). Left, potentiation of perforant path–evoked eEPSCs induced by high-frequency stimulation (HFS, indicated by arrow) in granule cells. Inset traces, representative traces of eEPSCs during 0.1-Hz frequency transmission before and after the induction of potentiation. Shown are eEPSCs recorded at 60 min after the HFS, normalized to the amplitude of the corresponding response in the baseline. Right, mean amplitudes of eEPSCs recorded from 50 to 60 min after HFS. *P < 0.05 (Student's t-test) (n = 3 for each group; both sexes at 8.5–9 months of age). (**j**) Passive avoidance test from wild-type and APP/PS1 mice with or without oral administration of selegiline. Left, experimental protocol for passive avoidance test. Right, latency to enter dark chamber during passive avoidance test for wild-type and APP/PS1 mice with or without oral administration of selegiline (10 mg kg^{-1} d^{-1} for 7 d, both sexes at 10–12 months of age). Two-way repeated-measures ANOVA revealed significant effects for the genotype ($F(1,42) = 18.630$, $P = 0.000$), significant effects for the drug ($F(1,42) = 12.494$, $P = 0.001$), without significant interaction effect between genotype and drug. ***P < 0.001, *P < 0.05 (Bonferroni's *post hoc* analysis). Number on each bar refers to the number of cells (**a**,**b**,**d**,**f**,**h**,**i**) and mice (**j**) analyzed. n refers to the number of animals tested. Each cell was recorded once for each stimulus intensity. Data are means ± s.e.m.

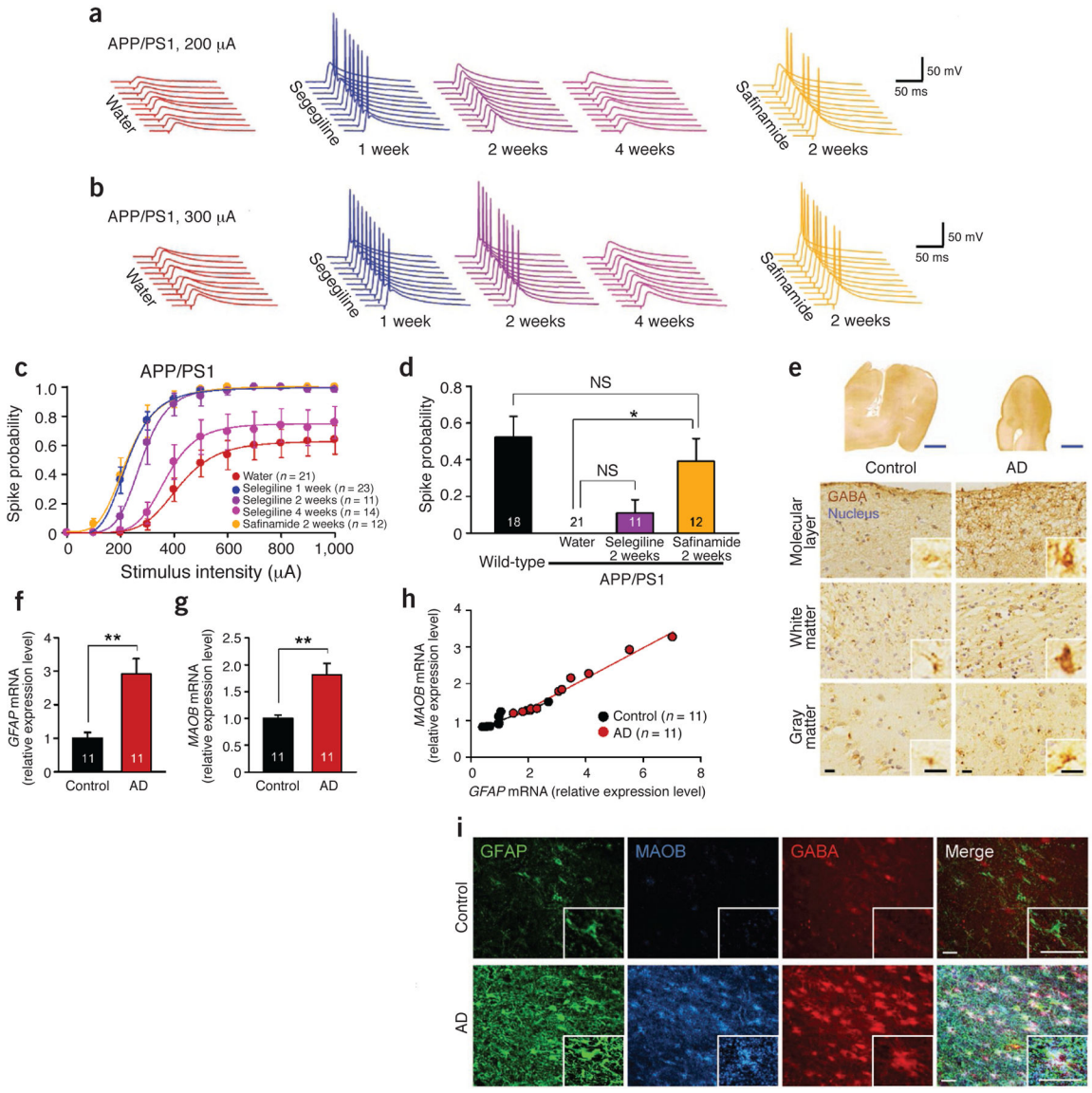

Figure 6.

Clinical relevance of GABA from reactive astrocytes. (**a**–**d**) Evoked spike probability by electrical stimulation of perforant path (0.1 Hz, 100 μs, 100–1,000 μA) (for selegiline 2 weeks and 4 weeks and safinamide 2 weeks, $n = 2$ mice for each group; both sexes at 10–12 months of age). Each cell was recorded once for each stimulus intensity. (**a**) Representative traces of evoked EPSPs with selegiline or safinamide (10 mg kg^{-1} d^{-1} oral administration) at 200-μA stimulation. (**b**) Representative traces of evoked EPSPs at 300 μA stimulation. (**c**) Summary graph of spike probability versus stimulus intensity. Water group is the same group from Figure 5f; selegiline 1-week group includes the 11 cells of the selegiline before group in Figure 5h. (**d**) Comparison of spike probability at 200-μA stimulation after 2 weeks of administration of Maob inhibitors. Wild-type group and Water group are the same groups from Figure 5f. One-way ANOVA and Scheffe's test; $*P < 0.05$. (**e**) Immunohistochemistry of GABA and hematoxylin-stained nuclei in the temporal cortex of human postmortem brain. Inset, magnified images. Blue scale bars, 5 mm; black scale bars, 15 μm. (**f**) Relative

expression level of *GFAP* mRNA measured by quantitative real-time PCR. $^{**}P < 0.01$ (Student's *t*-test). (**g**) Relative expression level of *MAOB* mRNA. $^{**}P < 0.01$ (Student's *t*-test). (**h**) Scatter plot shows positive correlation between *GFAP* and *MAOB* mRNA extent. Control: $r = 0.89$, $P < 0.0005$; subject with AD: $r = 0.99$, $P < 0.0001$ (simple correlation analysis). (**i**) Confocal images of GFAP, MAOB and GABA abundance. Inset, magnified images of AD and control astrocytes. Scale bars, 30 μm. Number on each bar refer to the number of cells (***c*,d**) or human cases (**f**–**h**) analyzed. Data are means ± s.e.m.